Classification: BIOLOGICAL SCIENCES; Biochemistry

Crystal structure and stability of gyrase-fluoroquinolone cleaved complexes from *M. tuberculosis*

Tim R. Blower[a,1], Benjamin H. Williamson[b], Robert J. Kerns[b] and James M. Berger[a,2]

[a]Johns Hopkins University School of Medicine, Department of Biophysics and Biophysical Chemistry, Baltimore, Maryland, 21205, USA

[b]Division of Medicinal and Natural Products Chemistry, University of Iowa, Iowa City, Iowa 52242, USA

[1]Current address: School of Biological and Biomedical Sciences and Department of Chemistry, Durham University, Durham, DH1 3LE, UK

[2]To whom correspondence may be addressed. Email: jmberger@jhmi.edu

KEYWORDS: *Mycobacterium tuberculosis*, antibiotic resistance, fluoroquinolone, gyrase

ABSTRACT

Mycobacterium tuberculosis (*Mtb*) infects one-third of the world's population, and in 2013 accounted for 1.5 million deaths. Fluoroquinolone antibacterials, which target DNA gyrase, are critical agents used to halt the progression from multidrug-resistant tuberculosis to extensively resistant disease; however, fluoroquinolone resistance is emerging and new ways to bypass resistance are required. To better explain known differences in fluoroquinolone action, the crystal structures of the wild-type *Mtb* DNA gyrase cleavage core and a fluoroquinolone-sensitized mutant were determined in complex with DNA and five fluoroquinolones. The structures, ranging from 2.4-2.6 Å resolution, show that the intrinsically low susceptibility of *Mtb* to fluoroquinolones correlates with a reduction in contacts to the water-shell of an associated magnesium ion, which bridges fluoroquinolone-gyrase interactions. Surprisingly, the structural data revealed few differences in fluoroquinolone-enzyme contacts from drugs that have very different activities against *Mtb*. By contrast, a stability assay using purified components showed a clear relationship between ternary complex reversibility and inhibitory activities reported with cultured cells. Collectively, our data indicate that the stability of fluoroquinolone/DNA interactions is a major determinant of fluoroquinolone activity, and that moieties which have been appended to the C7 position of different quinolone scaffolds do not take advantage of specific contacts that might be made with the enzyme. These concepts point to new approaches for developing quinolone-class compounds that have increased potency against *Mtb* and the ability to overcome resistance.

SIGNIFICANCE STATEMENT

Although tuberculosis is a curable disease, its etiological agent, *Mycobacterium tuberculosis* (*Mtb*), remains a major human pathogen. Control of *Mtb* is hindered by multidrug-resistant strains. These are currently treated with second-line agents including fluoroquinolones such as moxifloxacin, which is one of a powerful three-drug regimen in trials against *Mtb*. Unfortunately, fluoroquinolone resistance is increasing, making improvements to quinolone efficacy clinically important. Fluoroquinolones act by forming complexes that poison *Mtb*. This study describes the first X-ray crystal structures of the *Mtb* gyrase cleavage core complexed with DNA and five fluoroquinolones. These comparative structures inform efforts to design new quinolone-class agents and establish that the low intrinsic susceptibility of *Mtb* to clinically-used fluoroquinolones is due to a paucity of specific gyrase-drug interactions.

\body

INTRODUCTION

Mycobacterium tuberculosis (*Mtb*), the causative agent of tuberculosis (TB), is one of the most important pathogens of humans, second only to the human immunodeficiency virus in the number of deaths caused annually (1). *Mtb* is estimated to latently infect one-third of the world's population (2), thereby also creating a huge reservoir for future disease. Particularly problematic are cases of multidrug-resistant (MDR)-TB, which is defined as resistance to two primary anti-tuberculosis drugs, rifampicin and isoniazid. MDR-TB now represents 3.5 % of new TB cases; of these, 9 % are classified as extensively drug-resistant (XDR)-TB (1), which is defined as MDR-TB with additional resistance to any fluoroquinolone and one injectable second-line drug (3). TB isolates are also being recovered that are totally drug-resistant (3–5). Thus, controlling TB, in particular drug-resistant tuberculosis, is a major health problem.

Fluoroquinolones are one of the most successful classes of drug against bacterial pathogens, accounting for 24 % of the $10 billion US antibiotic market (6). Fluoroquinolones are also currently receiving considerable attention in the treatment of TB, with two new C8-methoxy derivatives, moxifloxacin and gatifloxacin, currently under evaluation as promising first-line therapeutics (7–10). These compounds have been used to restrict the development of XDR-TB from MDR-TB; however, emerging resistance threatens both first-line and second-line use (11). The widespread testing of fluoroquinolones against tuberculosis has revealed considerable variation in efficacy of different drug variants against *Mtb*. For example, ciprofloxacin is only marginally active, and its early use with *Mtb* was halted in favor of ofloxacin and levofloxacin (7). These two agents are now proving to be less effective than moxifloxacin and gatifloxacin (7, 10); however, the newest two compounds also exhibit some non-ideality. For example, gatifloxacin can elicit side-effects such as hypo/hyper-glycaemia (12), while moxifloxacin has potential cardiovascular risks (13). Although recent clinical trials that have included fluoroquinolones as part of an alternative drug-regimen have faltered (14),

there are prospects for other non-fluoroquinolone molecules to make an impact on the treatment of MDR- and XDR-TB (15, 16). Moreover, a promising recent trial, which uses moxifloxacin as part of a 3-drug regimen together with pretomanid and pyrazinamide (MPaZ), reports superior bactericidal activity against TB and MDR-TB versus current regimens (17). These new data make it clear that new quinolone-class agents, which are also capable of circumventing known resistance mutations, might be useful therapeutic agents in the treatment of TB.

Progress is presently being made toward developing new fluoroquinolone derivatives. For example, a methoxy group at fluoroquinolone position C8 (**Fig. 1A**) increases activity against mycobacteria, particularly resistant mutants (18–20). Indeed, moxifloxacin, along with a more active C8-methyl derivative, retain high inhibitory activity against purified *Mtb* gyrase even when the enzyme contains commonly acquired fluoroquinolone-resistance substitutions (see accompanying manuscript by Aldred *et al*). In another example, quinazolinediones (diones) have been shown to have an ability to bypass existing resistance within mycobacteria and other bacterial species (20–23). Thus, there still exist opportunities to design more effective quinolone-class molecules for treatment of TB.

DNA gyrase is a heterotetrameric ($GyrA_2GyrB_2$) enzyme that transiently catalyzes double-strand (ds) DNA breaks as it negatively supercoils DNA. Fluoroquinolones prevent the re-sealing of the ds breaks that normally follows DNA strand passage (24), generating persistent, covalent enzyme-DNA adducts called cleaved complexes. Cleaved-complex formation, which is reversible, blocks bacterial growth; at elevated fluoroquinolone concentrations, release of DNA breaks from the complexes leads to chromosome fragmentation and cell death (25). Although numerous crystallographic studies have defined the primary binding site of fluoroquinolones against gyrase (and against topoisomerase

97 IV, a gyrase paralog) (26–29), there has been debate as to whether fluoroquinolones use a
98 magnesium ion to bridge their interaction with the enzyme (27, 28). Resolving this question is
99 important, as the intrinsic resistance of certain species of gyrase to quinolones (e.g., *Mtb*) has been
100 proposed to result from natural sequence variation that leads to the loss of a magnesium-ion
101 "bridge" formed between the drug and enzyme (30–32). At the same time, there currently exists no
102 clear chemical explanation as to why certain fluoroquinolone derivatives act with different efficacies
103 against *Mtb* gyrase.

104

105 To better understand such questions, we carried out a structural and biochemical analysis of
106 *Mtb* gyrase in the presence of a panel of four different, clinically-used fluoroquinolones
107 (ciprofloxacin, levofloxacin, gatifloxacin and moxifloxacin) and one new fluoroquinolone derivative
108 (C8-Me-moxifloxacin). X-ray crystallography revealed that *Mtb* gyrase indeed makes an intrinsically
109 low number of interactions with a magnesium ion that accompanies fluoroquinolone binding, and
110 that the introduction of a drug-sensitizing mutation (GyrA A90S) restores interactions seen in non-
111 resistant gyrase homologs. *In vitro*, we find that C8-Me-moxifloxacin and moxifloxacin are most
112 effective at promoting cleaved complex formation and inhibiting DNA supercoiling by *Mtb* gyrase,
113 followed by gatifloxacin, and then ciprofloxacin and levofloxacin; however, crystal structures of the
114 DNA-binding-and-cleavage core of *Mtb* gyrase with both DNA and drug surprisingly failed to reveal
115 any substantial differences in the contacts formed between the protein and different drugs. Further
116 biochemical investigations using an assay that monitors the stability of pre-formed cleaved-
117 complexes largely corroborated the rank-order of inhibition seen in DNA cleavage experiments, and
118 moreover resulted in drug efficacy trends that closely accord with clinical effectiveness. Collectively,
119 our data explain why *Mtb* gyrase is naturally quinolone resistant and show that the relative activities
120 of existing panels of anti-TB quinolone therapeutics are heavily influenced by base-stacking

121 interactions and have yet to take advantage of direct gyrase contacts to maximize therapeutic
122 potential.
123

RESULTS

A C8-methyl derivative of moxifloxacin shows enhanced DNA cleavage with *Mtb* gyrase over clinically-used fluoroquinolones.

Mtb is well known to have a low susceptibility to fluoroquinolones (33, 34). For example, the wild-type minimal inhibitory concentration (MIC) for ciprofloxacin and levofloxacin is 20- and 140-fold higher, respectively, with *Mtb* than with *Escherichia coli* (30). Part of this innately low susceptibility has been proposed to arise from a natural variation in the Quinolone-Resistance Determining Region (QRDR) of the GyrA subunit of gyrase that substitutes an alanine (Ala90 in *Mtb*) for what is typically a serine at the second amino acid of helix α4. As a serine, this amino acid has been seen in some instances to participate in a water/magnesium ion bridge that connects the enzyme (topoisomerase IV or gyrase) to the fluoroquinolone (28) (interestingly, while biochemical studies have substantiated the importance of this interaction (35–38), magnesium ion binding has not been observed crystallographically in all instances, leading to some debate as to its relevance (27, 28). Acquired resistance also centers in general around the helix α4 region, with 54 % of 654 FQ-resistant isolates containing substitutions at residues 90, 91 and 94 of *Mtb* GyrA (11).

To begin to define how *Mtb* gyrase responds *in vitro* to different, clinically-tested fluoroquinolones, we first purified full-length *Mtb* GyrA and GyrB, using the new consensus 675-amino-acid form of GyrB (11, 39). To investigate *Mtb*'s innate fluoroquinolone insensitivity, an Ala90Ser (A90S) variant of *Mtb* GyrA, which has been predicted to aid in the formation of a water/magnesium ion bridge (31, 32), was also prepared. Wild-type (WT) *Mtb* GyrA and GyrA^{A90S} proteins were combined with WT *Mtb* GyrB to form active heterotetrameric enzymes. These enzymes were then used to assess the fluoroquinolone-dependent generation of cleaved complexes (**Fig. 1B**), as monitored by the formation of linearized DNA from a starting supercoiled plasmid. In

this assay, levofloxacin produced the lowest amount of linear product, with ciprofloxacin, gatifloxacin and moxifloxacin showing between 2- and 4-fold higher cleavage activities at 10 µM drug (**Fig. 1C *left panel***). By comparison, C8-Me-moxifloxacin produced 10-fold greater amounts of linearized DNA than levofloxacin at the same concentration (the level of activity for C8-Me-moxifloxacin is actually an underestimate of the compound's efficacy due to the formation of multiple cleaved complexes at drug concentrations >5 µM; the formation of multiple cleaved complexes on each DNA molecule degrades the linear product, artificially lowering the readout) (**Fig. 1B and C**). When compared under similar conditions, the GyrA^{A90S} form of *Mtb* gyrase consistently exhibited greater sensitivity to low fluoroquinolone concentrations than the WT enzyme (**Fig. 1C *right panel***); the relative drug activity trends seen in cleaved-complex assays with the WT and GyrA^{A90S} enzymes also were observed for the inhibition of ATP-dependent supercoiling (**Fig. S1**). Interestingly, a previous study testing each drug against *Mtb* in cell culture reported similar MIC values of 0.5 µg/ml for moxifloxacin, levofloxacin and ciprofloxacin, and a lower value of 0.1 µg/ml for gatifloxacin (31). This finding indicates that there is a disconnect in the rank-ordering drug of efficacy when using data obtained from MIC and from biochemical experiments. Nonetheless, the observed cleavage and supercoil-inhibition trends seen here are consistent with the observation that both ciprofloxacin and levofloxacin are less effective in the clinic than the fourth-generation fluoroquinolones gatifloxacin and moxifloxacin (7, 10).

Crystallization of *Mtb* gyrase-DNA-fluoroquinolone complexes.

To better understand structure-activity relationships that underlie the different activities of fluoroquinolones, both amongst themselves and against *Mtb*, we set out to solve the structure of *Mtb* gyrase bound to ciprofloxacin, levofloxacin, gatifloxacin, moxifloxacin, and C8-Me-moxifloxacin with DNA. Following a strategy that worked previously for *Staphylococcus aureus* gyrase (29), we linked the C-terminal region of GyrB (residues 426-675) and the N-terminal region of GyrA (residues

2-500) into a single polypeptide chain (termed GyrBA). In parallel, a GyrA^{A90S} variant of this construct was also prepared. The *in vitro* activity of the WT and mutant *Mtb* GyrBA fusions was confirmed by monitoring the cleavage of a supercoiled substrate in the presence of each of the five fluoroquinolones (**Fig. S2A**). Each drug induced DNA cleavage by the fusion protein (**Fig. S2B *left panel***) and, as with full-length gyrase, cleavage was enhanced by the A90S substitution (**Fig. S2B *right panel***).

For crystallization, the fusion proteins were mixed with fluoroquinolone and a 24-mer dsDNA substrate, using an oligonucleotide sequence that had been previously crystallized with moxifloxacin and *Acinetobacter baumannii* topo IV (28). Following screening and refinement of crystallization conditions, we obtained the best data from co-crystals of the *Mtb* GyrBA^{WT} fusion combined with both DNA and moxifloxacin, which diffracted to 2.4 Å. An initial solution was obtained for this complex by molecular replacement using a search model comprising only the protein and DNA from a previous, moxifloxacin-containing cleaved-complex structure (*A. baumannii* topo IV, PDB: 2XKK) (28). Having built and finalized this first structure, the protein and DNA from the *Mtb* gyrase model (without the drug) were subsequently used as a search model for all remaining cleaved-complex structures. In this manner, structures were obtained from 2.4 to 2.6 Å resolution for both the GyrBA^{WT} and GyrBA^{A90S} fusions in complex with moxifloxacin, C8-Me-moxifloxacin, gatifloxacin, and levofloxacin (**Table S1**). For ciprofloxacin, only the GyrBA^{A90S} fusion formed crystals that diffracted to better than 3 Å resolution; the GyrBA^{WT} crystal form showed consistently weak diffraction (>4 Å) and was not analyzed further.

Structure of *Mtb* DNA gyrase in complex with DNA and moxifloxacin.

Inspection of the moxifloxacin-bound GyrBA^{WT} structure shows that, as with other bacterial type IIA topoisomerase-DNA complexes (26–29), the *Mtb* gyrase cleavage core binds a single dsDNA within a channel that spans the dimer interface (**Fig. 2A**). The dsDNA is kinked at two points by the intercalation of Ile181 from GyrA into the minor groove, generating an upwardly curved duplex. Each strand is cleaved once, with the 5'-phosphate of each cleaved strand covalently attached to one catalytic tyrosine (Tyr129) in each of the two GyrA regions (**Fig. S3A**). The presence of clear electron density allowed for the modeling of two moxifloxacin molecules, each wedged between the two ends of the cleaved DNA strands on both halves of the complex (**Fig. 2B; Fig. S3A and B**), in a drug-binding pocket whose walls are formed by DNA base stacking. The orientation of moxifloxacin was immediately evident from electron density features, which also unequivocally showed that a magnesium ion was coordinated by the keto-acid group of each quinolone core (**Fig. S3B**). A GyrA dimerization interface (the "C-gate"), which is formed by a pair of coiled-coil arms extending from the principal DNA binding platform, was closed in the moxifloxacin-bound complex (**Fig. 2C and D**); this region has been seen in different conformational states in other type IIA topoisomerase structures (40, 41). A single magnesium ion and several associated waters are present in each of the two active sites at the so-called "B" (non-catalytic) position (42), coordinated by Glu459, Asp532, and Asp534 of GyrB (**Fig. S3C**).

Comparison of the *Mtb* DNA- and fluoroquinolone-bound cleavage core with a previously determined apo structure of the N-terminal portion of *Mtb* GyrA (43) revealed two modest structural differences in the active site. First, a flexible loop from the apo structure (Ser178-Ile187) swings into a new position in the cleaved complex, forming two β-strands joined by a short turn (**Fig. S4A**). This β-sheet creates a portion of the DNA-binding surface and specifically presents GyrA-Ile181 for intercalating into and bending DNA (**Fig. S4A**). Second, in its apo form, GyrA-Asp89 lies at the end

of a loop where it would form unfavorable contacts with an incoming fluoroquinolone (Fig. S4B); in the complex, Asp89 initiates helix α4 of GyrA, and the acidic side chain is rotated away from the keto-acid group of the fluoroquinolone to position Ala90 near the bound drug (Fig. S4B). The gyrase nucleolytic center thus undergoes multiple local movements that are likely important for allowing both enzymatic and drug-binding activities.

Mtb gyrase naturally lacks reinforcing contacts to the water/magnesium ion bridge that are present in sensitized homologs.

Examination of the region surrounding the keto-acid moiety of moxifloxacin bound to WT *Mtb* gyrase reveals a defined network of hydrogen bonds that link moxifloxacin, through a hydrated magnesium ion, to GyrA (Fig. 3B; Fig. S5A). In each model, two or three of the water molecules coordinating the drug-bound magnesium ions were clearly visible within the electron density (Fig. S5A and B) (additional waters were then placed to complete the octahedral coordination sphere commonly observed with magnesium ions (44) and within crystal structures of individual quinolones (45)). One notable, water-mediated magnesium-ion contact is with Asp94 of GyrA; this interaction likely accounts for why many substitutions at Asp94 lead to drug insensitivity in fluoroquinolone-resistant laboratory and clinical strain isolates (11, 46) (see also accompanying manuscript by Aldred *et al.*). Comparison of the WT and A90S structures revealed that the hydroxyl from Ser90 also directly contacts magnesium ion-associated waters, as well as the quinolone keto-acid group directly (Fig. 3C; Fig. S5B). The absence of these contacts in the $GyrBA^{WT}$ structure accords with biochemical results showing that the natural presence of alanine at position 90 is at least partly responsible for the innately reduced susceptibility of the *Mtb* enzyme to fluoroquinolones, compared to homologs that retain a serine (or threonine, or asparagine) at this site (Fig. S5C) (30–32).

Diverse fluoroquinolones show few differences in binding interactions with the cleavage core of *Mtb* DNA gyrase.

Having established the moxifloxacin-inhibited GyrBA^{WT} and GyrBA^{A90S} structures as a starting point for our investigations of fluoroquinolone mechanism, we next determined and examined the structures of the other fluoroquinolone-inhibited complexes. Globally, no large conformational changes were seen between the moxifloxacin-bound complex and all subsequent complexes. Simulated annealing omit maps (47) were generated for each of the ternary complex structures to confirm the correct fit of each fluoroquinolone with its associated magnesium ion and coordinating waters (**Fig. 4**). Identification of the fluoroquinolone N1 cyclopropyl and C8 group orientations was unequivocal (in the case of levofloxacin, the fused ring structure was clearly observed). The N1 cyclopropyl and C8 methoxy groups of moxifloxacin and gatifloxacin adopt a *trans* configuration that extends out of the plane of the core ring structure, as predicted by energy minimization (48); the C8-methyl of C8-Me-moxifloxacin remains in plane with the ring (**Fig. 4**). In comparison to the fluoroquinolone N1 and C8 groups, the C7 groups (which distinguish all of the drug variants examined here except moxifloxacin and C8-Me-moxifloxacin) were less well defined (**Fig. 4**). This observation suggests that these C7 moieties exhibit a degree of innate flexibility within cleaved-complexes. The residues neighboring each C7 group – Arg482, Thr500, and Glu501 of GyrB – varied little in their relative positions, and made no specific contacts with the C7 group of any fluoroquinolone analyzed here. The unsubstituted C7 piperazinyl ring of ciprofloxacin resides > 4.2 Å from these neighboring residues, whereas the singly substituted rings in levofloxacin and gatifloxacin are within 3.4 Å and 3.8 Å of the same amino acids. Levofloxacin and gatifloxacin, together with both moxifloxacin compounds (which have larger C7 groups), thus are within the van der Waals contact radius of residues around the C7 ring, although these interactions appear generally loose and non-specific (**Fig. 4**).

269 The corresponding *Mtb* structures were next aligned to the structures of type IIA
270 topoisomerases from other bacterial species previously reported for cleaved complexes containing
271 moxifloxacin (28), ciprofloxacin (29), and levofloxacin (27) (**Figs. 4B, C and E, respectively**). In each
272 case, there did not appear to be any residues capable of making specific drug-protein contacts
273 outside of the water/magnesium-ion bridge network. Interestingly, fluoroquinolone-resistant clinical
274 isolates have been found with amino acid substitutions located around the C7 interaction locus of
275 *Mtb* GyrB (Thr500 to Asn/Pro and Glu501 to Asp/Val) (11). Thus, GyrB residues in this region appear
276 to form a favorable non-specific environment for hosting C7 groups that have been used in
277 therapeutically-approved fluoroquinolones, rather than a tailored set of contacts that can interact
278 with and potentially distinguish such drugs.

279

280 **Stability of *Mtb* gyrase-DNA-fluoroquinolone complexes correlates with activity.**

281 Altogether, the structural data on different *Mtb* GyrBA•DNA•drug complexes failed to show clear
282 differences in the types of protein-drug interactions seen for the panel of five fluoroquinolones
283 tested. While comparative MIC determinations have suggested that ciprofloxacin (0.5 μg/ml),
284 levofloxacin (0.5 μg/ml) and moxifloxacin (0.5 μg/ml) are equally effective against *Mtb*, and that this
285 correlates approximately with supercoiling inhibition, this trend did not correlate well with
286 previously-reported cleavage assays (31) or our own biochemical data (**Figs. 1 and S1**). We therefore
287 elected to search for another measure of drug activity other than formation of cleavage complexes
288 and supercoiling inhibition that might help explain this disconnect.

289

290 Because cleaved complex formation is reversible (49), one can assess the relative stability of
291 fluoroquinolone-poisoned gyrase•DNA adducts in solution (**Fig. 5**). In this approach, cleaved
292 complexes are first generated with full-length gyrase, followed by their dilution into buffer

containing no drug (to lower the concentration of the compound). DNA resealing is then assessed by the loss of linear product over time using agarose gel electrophoresis (36). When starting at the same drug concentration (20 μM), ciprofloxacin provided the shortest half-life for cleaved-complex reversal (0.4 h), followed by levofloxacin (0.6 h), gatifloxacin (2.5 h), and then moxifloxacin (3.0 h) (**Fig. 5A and C**). Interestingly, under these initial assay conditions, it was not possible to measure the persistence of complexes formed with C8-Me-moxifloxacin because the DNA was heavily degraded by the robust ability of the compound to stimulate multiple cleavage events. We therefore lowered the initial inhibitor concentration 4-fold (to 5 μM), shortened the incubation step, and again compared the parent moxifloxacin with its C8-methyl derivative. Under these conditions, the half-life for moxifloxacin was 0.9 h and 6.2 h for C8-Me-moxifloxacin (**Fig. 5B and D**). The GyrA A90S substitution further increased the stability of these complexes, raising the half-life of the moxifloxacin complex by 7-fold (to 7.0 h); under these conditions, the C8-Me-moxifloxacin complexes showed virtually no reversal. Thus, the observed order of fluoroquinolone activity seen within clinical studies (2, 7, 10), correlates most closely with the relative stabilities of the cleaved-complexes formed by these agents.

DISCUSSION

We have determined the crystal structures of nine different fluoroquinolone•enzyme•DNA complexes for *M. tuberculosis* gyrase. Overall, the structures, which offer the highest resolution yet obtained for such complexes, are generally similar to those seen previously for other fluoroquinolone-inhibited type IIA topoisomerase structures (27–29): each GyrBA core binds and cleaves a single DNA duplex, and one fluoroquinolone stacks between each of the two base pairs that flank the sites of cleavage. In accord with gyrase and topo IV structures from *Staphylococcus aureus* and *Acinetobacter baumannii*, respectively (28, 29), a single water/magnesium-ion network can be seen to link each drug to a portion of helix α4 of GyrA, supporting biochemical studies implicating this feature as a key facet of fluoroquinolone/gyrase interactions. The structures corroborate previous predictions as to why *Mtb* has an innately low susceptibility to fluoroquinolones (30–32), showing that Ala90 of GyrA (which is a serine in most gyrase and topo IV orthologs) cannot participate in stabilizing this ion-bridging network (**Fig. 3**). The importance of the magnesium-ion interaction has been further demonstrated by studies of the *Mtb* fluoroquinolone-resistance mutation GyrA^{A90V} (see accompanying manuscript by Aldred *et al*.), which from our structures, would be predicted to sterically block formation of the water/magnesium bridge. Given that acquired fluoroquinolone resistance in clinical isolates of *Mtb* tends to cluster in amino acids participating in the water/magnesium bridge (11), our structures indicate that any change to this region likely will alter the overall shape complementarity of the drug pocket, potentially explaining the protective nature of other substitutions in the helix α4 region (such as GyrA^{G88C}) that have been observed in experiments using cultured cells (20).

The present work is significant in that it assesses for the first time how five structurally different fluoroquinolones – ciprofloxacin, levofloxacin, gatifloxacin, moxifloxacin, and C8-Me-moxifloxacin – all interact with a single topoisomerase target. Surprisingly, we could identify no

specific interactions between the different fluoroquinolones and gyrase that might account for established differences in their anti-bacterial activities *in vivo* (2, 7, 10). Structural comparisons indicate that this paucity of enzyme-drug interactions is characteristic of cleaved complexes involving other bacterial type IIA topoisomerases (**Fig. 4**). Despite this finding, the activities of the compounds can be biochemically rank-ordered with their relative *in vivo* efficacies by assessing the relative stabilities of cleaved-complexes in solution (C8-Me-moxifloxacin > moxifloxacin > gatifloxacin > levofloxacin > ciprofloxacin) (**Fig. 5**). This overall efficacy ranking is similar to that derived from assays that monitor cleaved-complex formation or supercoil formation, with the exception of levofloxacin and ciprofloxacin: in our hands, levofloxacin appeared more capable of stabilizing cleaved-complexes than ciprofloxacin (**Fig. 5**), but less capable of forming such complexes or inhibiting DNA supercoiling (**Figs. 1 and S1**). The more effective drugs such as C8-Me-moxifloxacin, moxifloxacin and gatifloxacin demonstrated the highest levels of supercoiling inhibition and DNA cleavage, implying that the catalytic rate of DNA cleavage is higher with these compounds. As enzyme inhibition is then maintained through increased cleaved complex stability, the catalytic rate for strand passage and re-sealing of dsDNA breaks would be reduced. Our data, however, show that this model requires refinement. Although levofloxacin showed lower levels of supercoiling inhibition in comparison to ciprofloxacin, this compound's cleaved complexes were more stable. Nevertheless, cleaved-complex stability correlates well with *in vivo* efficacy and is likely to relate to the killing of *Mtb* cells; this hypothesis is supported by previous data showing how complex stability is a determining factor for the cytotoxicity of topoisomerase poisons within eukaryotic cells (50).

The fact that drug structure affects the formation and reversal of cleaved complexes in a manner that cannot immediately be tied to observable differences in protein-fluoroquinolone interactions implies that some more subtle chemical feature of the compounds – such as electronic charge distribution or DNA base stacking – plays a key role in determining fluoroquinolone potency. Stacking interactions are likely to be defined by electron localization within the quinolone/dione core, which in turn may be influenced by ancillary C7 and C8 groups. The robust improvement of C8-

Me-moxifloxacin activity compared to the C8-methoxy substituent in moxifloxacin alone highlights the power of fine-tuning the chemistry around the drug core. We hypothesize that the approximate 7-fold increase in stability of the C8-Me-moxifloxacin cleavage complex over the moxifloxacin cleavage complex might be linked in part to an increase in movement by the C7-diazabicyclo ring within C8-Me-moxifloxacin. In moxifloxacin, the N1 cyclopropyl and C8 methoxy groups were predicted (48) and indeed crystallized in *trans*, with the methoxy positioned to potentially interact with the C7 ring (**Fig. 4**). Without this methoxy oxygen, the C7-diazabicyclo ring of C8-Me-moxifloxacin may more freely rotate, and together with the absence of the oxygen atom, this may allow for new electronic charge distributions to form compared with moxifloxacin, resulting in altered base stacking and a more stable complex. Unfortunately for design efforts, stacking energetics are notoriously difficult to predict from structures. Stacking energetics can also be difficult to modulate through structure-based drug design approaches (51, 52), which struggle with the accurate accounting of factors such as flexibility or the entropy of drug binding (53). Further stability assays will be required to assess other substitutions at C8.

The inability of different C7 substituents from the panel of fluoroquinolones tested here to make specific interactions with GyrB is notable. The C7 group of each tested fluoroquinolone is surrounded by the QRDR of GyrB (54) (**Fig. 4**). Amino acid substitutions within the QRDR can produce acquired resistance; however, of sequenced fluoroquinolone-resistant isolates, only 3 % carry substitutions within the QRDR of GyrB compared with 64 % within the QRDR of GyrA (11). In *Mtb*, GyrB resistance substitutions include Asn499Lys/Thr, Thr500Asn/Pro, and Glu501Asp/Val (11). None of these residues in GyrB are sufficiently close to form specific contacts with even the largest C7 group tested (moxifloxacin) (**Fig. 4**). Instead, the structural data indicate that the QRDR of GyrB provides a complementary van der Waals surface that can favorably accommodate fairly large moieties and, together with a solvent exposed region above the C7 groups, that can allow for a

385 degree of conformational freedom for groups localized to this region. Much attention has already
386 been paid to modifying C7 ring groups, with clear success (22, 48, 55); it seems likely that these
387 improvements could be further capitalized upon by using longer linkers at the C7 position and
388 allowing substituents to reach and contact side chains of amino acids such as Arg482, Thr500, or
389 Glu501 in a more specific manner. In such an approach, it might be possible to pin a fluoroquinolone
390 in the gyrase drug-binding pocket, using a water/magnesium-ion bridge from GyrA to anchor the
391 keto-acid group at one end of the drug and specific contacts from GyrB to C7 features at the other;
392 indeed, crosslinks can be formed between the C7 end of ciprofloxacin and GyrB-Glu466 of *E. coli*
393 gyrase (equivalent to *Mtb* GyrB-Glu501) (49). This feature may be important for designing not only
394 more active fluoroquinolones, but also more active quinazolinediones (56).

395

396 The fluoroquinolone scaffold remains an important starting point for new antibiotics (57–
397 59). Indeed, both moxifloxacin (and in particular a new C8-Me-moxifloxacin derivative) retain high
398 inhibitory activity in cell-free assays that employ *Mtb* gyrase with commonly acquired
399 fluoroquinolone resistance substitutions (see accompanying manuscript by Aldred *et al*.).
400 Moxifloxacin has also been shown to maintain efficacy against acquired fluoroquinolone resistance
401 in a murine infection model of XDR strains (60). Data presented here indicate that fluoroquinolone
402 development should aim not just for increasing specific drug/enzyme interactions, but also for
403 integrating these efforts with investigations of the effects of drug variants on the stability of cleaved
404 complexes; one such approach would be to combine structure-based drug design with structure-
405 activity relationship studies and cleaved-complex reversal assays. A challenge to such efforts will be
406 to avoid the sole use of MIC as a means to score compound efficacy, and instead focus on cell killing,
407 which mitigates resistance (61). A second will be to augment the anti-gyrase and anti-bacterial
408 potency of new compounds while mitigating non-specific DNA intercalation and crossover against
409 the human gyrase homologs, topo IIα and topo IIβ.

410

MATERIALS AND METHODS

Reagents. Ciprofloxacin-HCl salt, levofloxacin and moxifloxacin were obtained from Sigma-Aldrich. Gatifloxacin was obtained from Toronto Research Chemicals Inc. C8-Me-moxifloxacin was synthesized as described previously (37). Ciprofloxacin-HCl was dissolved in water; levofloxacin, moxifloxacin and C8-Me-moxifloxacin were all dissolved in DMSO; gatifloxacin was dissolved in HCl-acidified DMSO (pH ~6) to 8 mM. With the exception of gatifloxacin, all drug solutions were dissolved to 20 mM and all final solutions were stored at -80 °C during experimentation.

Preparation of plasmid DNA substrates. Negatively supercoiled pSG483 (2927 bp), a pBlueScript II SK+ (Agilent) derivative containing a *Bbv*CI site, was prepared from *E. coli* XL-1 blue cells (Agilent) using a maxiprep kit (Macherey-Nagel). Relaxed pSG483 DNA was prepared by nicking the negatively supercoiled substrate with Nb.*Bbv*CI (NEB), ligating with T4 DNA ligase (NEB), and purifying by ethanol precipitation.

DNA assays. Full details of DNA supercoiling and DNA cleavage assays can be found in SI Materials and Methods. The stability assays were performed as follows, using a protocol adapted from previous examples (35, 62) (see also accompanying manuscript by Aldred *et al*.). Initial reaction mixtures were set up as per the DNA cleavage assays, except each 20 µL reaction contained 1 µM of gyrase heterotetramers and 100 nM of negatively supercoiled pSG483. In one set of reactions, ciprofloxacin, levofloxacin, gatifloxacin, and moxifloxacin were present at 20 µM; in a second set, C8-Me-moxifloxacin and moxifloxacin were used at 5 µM. The first (high drug concentration) set was incubated at 37 °C for 1 h, whereas the second (low concentration) set was incubated for 30 min. After incubation, 1 µL of the reaction was taken as a “pre-dilution” sample and quenched with stopping buffer. Reactions were then diluted 20-fold by addition of 380 µL pre-warmed reaction buffer. 20 µL samples were taken at time points up to 7 h post-dilution, with the first sample taken

436 immediately after dilution (approximately 5-10 s) to represent the zero-hour time point. Samples
437 were added directly to stopping buffer, and they were processed and analyzed as per the DNA
438 supercoiling assays. Stability was measured by determining the loss of linear product over time
439 compared to 100 % linear product set by the zero-hour time point. Gel images were analyzed using
440 ImageJ (63), and data were plotted using Prism (GraphPad Software). Approximate half-lives were
441 calculated using the non-linear regression “one phase decay” mode of Prism (GraphPad Software).

442

443 **Protein expression and cleavage complex structure determination.** Full details concerning cloning,
444 protein expression and purification, complex crystallization, X-ray data collection and structure
445 determination can be found in SI Materials and Methods.

446

ACKNOWLEDGEMENTS

We thank Dr. Jon Schuermann (NE-CAT, Advanced Photon Source, Illinois) and Dr. Craig Ogata (GM/CA@APS, Advanced Photon Source, Illinois) for advice during data collection, Alexia Miller for *in silico* modelling support, Dr. Matthew Kitching (University of Manchester, UK) for expertise on drug molecules and figures, and Prof. Karl Drlica for extensive advice and critical reading of the manuscript. This work was supported by research grants from the NIH (AI87671, to RJK) and the National Cancer Institute of the NIH (R01-CA077373, to JMB). TRB was supported by a European Molecular Biology Organization Long-Term Fellowship. This work is based in part upon research conducted at the NE-CAT beamlines, which are funded by the National Institute of General Medical Sciences from the NIH (P41 GM103403). The Pilatus 6M detector on 24-ID-C beam line is funded by a NIH-ORIP HEI grant (S10 RR029205). This work is also based in part upon research conducted at the GM/CA@APS beamlines, which have been funded in whole or in part with Federal funds from NCI (ACB-12002) and NIGMS (AGM-12006). This research used resources of the Advanced Photon Source, a U.S. Department of Energy (DOE) Office of Science User Facility operated for the DOE Office of Science by Argonne National Laboratory under Contract No. DE-AC02-06CH11357.

DATA DEPOSITION

The atomic coordinates have been deposited in the Protein Data Bank, www.pdb.org (PDB ID codes 5BS8, 5BTA, 5BTC, 5BTD, 5BTF, 5BTG, 5BTI, 5BTL, 5BTN).

REFERENCES

1. World Health Organization (2014) Global Tuberculosis Report 2014. *World Heal Organ Geneva, Switz*.

2. Ginsburg AS, Grosset JH, Bishai WR (2003) Fluoroquinolones, tuberculosis, and resistance. *Lancet Infect Dis* 3(7):432–442.

3. Migliori GB, et al. (2012) Totally drug-resistant and extremely drug-resistant tuberculosis: the same disease? *Clin Infect Dis* 54(9):1379–80.

4. Velayati AA, et al. (2009) Emergence of new forms of totally drug-resistant tuberculosis bacilli: super extensively drug-resistant tuberculosis or totally drug-resistant strains in iran. *Chest* 136(2):420–5.

5. Gandhi NR, et al. (2010) Multidrug-resistant and extensively drug-resistant tuberculosis: a threat to global control of tuberculosis. *Lancet* 375(9728):1830–43.

6. Suda KJ, Hicks LA, Roberts RM, Hunkler RJ, Danziger LH (2013) A national evaluation of antibiotic expenditures by healthcare setting in the United States, 2009. *J Antimicrob Chemother* 68(3):715–8.

7. Takiff H, Guerrero E (2011) Current prospects for the fluoroquinolones as first-line tuberculosis therapy. *Antimicrob Agents Chemother* 55(12):5421–9.

8. Conde MB, et al. (2009) Moxifloxacin versus ethambutol in the initial treatment of tuberculosis: a double-blind, randomised, controlled phase II trial. *Lancet* 373(9670):1183–1189.

9. Grosset JH, Singer TG, Bishai WR (2012) New drugs for the treatment of tuberculosis: hope and reality. *Int J Tuberc Lung Dis* 16(8):1005–1014.

10. Blumberg HM, et al. (2003) American Thoracic Society/Centers for Disease Control and Prevention/Infectious Diseases Society of America: treatment of tuberculosis. *Am J Respir Crit Care Med* 167(4):603–62.

11. Maruri F, et al. (2012) A systematic review of gyrase mutations associated with fluoroquinolone-resistant Mycobacterium tuberculosis and a proposed gyrase numbering system. *J Antimicrob Chemother* 67(4):819–31.

12. Park-Wyllie LY, et al. (2006) Outpatient gatifloxacin therapy and dysglycemia in older adults. *N Engl J Med* 354(13):1352–61.

13. Koul A, Arnoult E, Lounis N, Guillemont J, Andries K (2011) The challenge of new drug discovery for tuberculosis. *Nature* 469(7331):483–90.

14. Lanoix J-P, Chaisson RE, Nuermberger EL (2015) Shortening tuberculosis treatment with fluoroquinolones: lost in translation? *Clin Infect Dis*. doi:10.1093/cid/civ911.

15. Brigden G, Hewison C, Varaine F (2015) New developments in the treatment of drug-resistant tuberculosis: clinical utility of bedaquiline and delamanid. *Infect Drug Resist* 8:367–378.

16. Lee H, Suh J-W (2015) Anti-tuberculosis lead molecules from natural products targeting Mycobacterium tuberculosis ClpC1. *J Ind Microbiol Biotechnol*. doi:10.1007/s10295-015-1709-3.

17. Dawson R, et al. (2015) Efficiency and safety of the combination of moxifloxacin, pretomanid (PA-824), and pyrazinamide during the first 8 weeks of antituberculosis treatment: a phase 2b, open-label, partly randomised trial in patients with drug-susceptible or drug-resistant pul. *Lancet (London, England)* 385(9979):1738–47.

18. Dong Y, Xu C, Zhao X, Domagala J, Drlica K (1998) Fluoroquinolone Action against Mycobacteria: Effects of C-8 Substituents on Growth, Survival, and Resistance. *Antimicrob Agents Chemother* 42(11):2978–2984.

19. Sindelar G, et al. (2000) Mutant Prevention Concentration as a Measure of Fluoroquinolone Potency against Mycobacteria. *Antimicrob Agents Chemother* 44(12):3337–3343.

20. Malik M, et al. (2011) Fluoroquinolone and quinazolinedione activities against wild-type and gyrase mutant strains of Mycobacterium smegmatis. *Antimicrob Agents Chemother* 55(5):2335–43.

21. Huband MD, et al. (2007) In vitro and in vivo activities of PD 0305970 and PD 0326448, new bacterial gyrase/topoisomerase inhibitors with potent antibacterial activities versus multidrug-resistant gram-positive and fastidious organism groups. *Antimicrob Agents Chemother* 51(4):1191–201.

22. German N, Malik M, Rosen JD, Drlica K, Kerns RJ (2008) Use of gyrase resistance mutants to guide selection of 8-methoxy-quinazoline-2,4-diones. *Antimicrob Agents Chemother* 52(11):3915–21.

23. Pan XS, Gould KA, Fisher LM (2009) Probing the differential interactions of quinazolinedione PD 0305970 and quinolones with gyrase and topoisomerase IV. *Antimicrob Agents Chemother* 53(9):3822–3831.

24. Aldred KJ, Kerns RJ, Osheroff N (2014) Mechanism of quinolone action and resistance. *Biochemistry* 53(10):1565–74.

25. Drlica K, Malik M, Kerns RJ, Zhao X (2008) Quinolone-mediated bacterial death. *Antimicrob Agents Chemother* 52(2):385–92.

26. Laponogov I, et al. (2009) Structural insight into the quinolone-DNA cleavage complex of type IIA topoisomerases. *Nat Struct Mol Biol* 16(6):667–669.

27. Laponogov I, et al. (2010) Structural basis of gate-DNA breakage and resealing by type II topoisomerases. *PLoS One* 5(6):e11338.

28. Wohlkonig A, et al. (2010) Structural basis of quinolone inhibition of type IIA topoisomerases and target-mediated resistance. *Nat Struct Mol Biol* 17(9):1152–1153.

29. Bax BD, et al. (2010) Type IIA topoisomerase inhibition by a new class of antibacterial agents. *Nature* 466(7309):935–940.

30. Guillemin I, Jarlier V, Cambau E (1998) Correlation between Quinolone Susceptibility Patterns and Sequences in the A and B Subunits of DNA Gyrase in Mycobacteria. *Antimicrob Agents Chemother* 42(8):2084–2088.

31. Aubry A, Pan X-S, Fisher LM, Jarlier V, Cambau E (2004) Mycobacterium tuberculosis DNA gyrase: interaction with quinolones and correlation with antimycobacterial drug activity. *Antimicrob Agents Chemother* 48(4):1281–8.

32. Matrat S, Aubry A, Mayer C, Jarlier V, Cambau E (2008) Mutagenesis in the alpha3alpha4 GyrA helix and in the Toprim domain of GyrB refines the contribution of Mycobacterium tuberculosis DNA gyrase to intrinsic resistance to quinolones. *Antimicrob Agents Chemother* 52(8):2909–14.

33. Morris RP, et al. (2005) Ancestral antibiotic resistance in Mycobacterium tuberculosis. *Proc Natl Acad Sci U S A* 102(34):12200–5.

34. Piton J, et al. (2010) Structural insights into the quinolone resistance mechanism of Mycobacterium tuberculosis DNA gyrase. *PLoS One* 5(8):e12245.

35. Aldred KJ, et al. (2012) Drug interactions with Bacillus anthracis topoisomerase IV: biochemical basis for quinolone action and resistance. *Biochemistry* 51(1):370–81.

36. Aldred KJ, McPherson SA, Turnbough CL, Kerns RJ, Osheroff N (2013) Topoisomerase IV-quinolone interactions are mediated through a water-metal ion bridge: mechanistic basis of quinolone resistance. *Nucleic Acids Res* 41(8):4628–4639.

595

596 37. Aldred KJ, et al. (2013) Overcoming target-mediated quinolone resistance in topoisomerase
597 IV by introducing metal-ion-independent drug-enzyme interactions. *ACS Chem Biol*
598 8(12):2660–8.
599

600 38. Aldred KJ, et al. (2014) Role of the water-metal ion bridge in mediating interactions between
601 quinolones and Escherichia coli topoisomerase IV. *Biochemistry* 53(34):5558–67.
602

603 39. Karkare S, Brown AC, Parish T, Maxwell A (2013) Identification of the likely translational start
604 of Mycobacterium tuberculosis GyrB. *BMC Res Notes* 6:274.
605

606 40. Dong KC, Berger JM (2007) Structural basis for gate-DNA recognition and bending by type IIA
607 topoisomerases. *Nature* 450(7173):1201–1205.
608

609 41. Wendorff TJ, Schmidt BH, Heslop P, Austin CA, Berger JM (2012) The Structure of DNA-Bound
610 Human Topoisomerase II Alpha: Conformational Mechanisms for Coordinating Inter-Subunit
611 Interactions with DNA Cleavage. *J Mol Biol*. doi:S0022-2836(12)00581-5
612 [pii]10.1016/j.jmb.2012.07.014.
613

614 42. Schmidt BH, Burgin AB, Deweese JE, Osheroff N, Berger JM (2010) A novel and unified two-
615 metal mechanism for DNA cleavage by type II and IA topoisomerases. *Nature* 465(7298):641–
616 644.
617

618 43. Tretter EM, Schoeffler AJ, Weisfield SR, Berger JM (2010) Crystal structure of the DNA gyrase
619 GyrA N-terminal domain from Mycobacterium tuberculosis. *Proteins* 78(2):492–495.
620

621 44. Bock CW, Kaufman A, Glusker JP (1994) Coordination of water to magnesium cations. *Inorg*
622 *Chem* 33(3):419–427.
623

624 45. Drevensek P, et al. (2006) X-Ray crystallographic, NMR and antimicrobial activity studies of
625 magnesium complexes of fluoroquinolones - racemic ofloxacin and its S-form, levofloxacin. *J*
626 *Inorg Biochem* 100(11):1755–63.
627

628 46. Zhou J, et al. (2000) Selection of antibiotic-resistant bacterial mutants: allelic diversity among
629 fluoroquinolone-resistant mutations. *J Infect Dis* 182(2):517–25.
630

631 47. Hodel A, Kim SH, Brünger AT (1992) Model bias in macromolecular crystal structures. *Acta*
632 *Crystallogr Sect A Found Crystallogr* 48(6):851–858.
633

634 48. Malik M, et al. (2010) Effect of N-1/c-8 ring fusion and C-7 ring structure on fluoroquinolone
635 lethality. *Antimicrob Agents Chemother* 54(12):5214–21.
636

637 49. Mustaev A, et al. (2014) Fluoroquinolone-gyrase-DNA complexes: two modes of drug binding.
638 *J Biol Chem* 289(18):12300–12.
639
640 50. Bandele OJ, Osheroff N (2008) The efficacy of topoisomerase II-targeted anticancer agents
641 reflects the persistence of drug-induced cleavage complexes in cells. *Biochemistry*
642 47(45):11900–8.
643
644 51. Anderson AC (2003) The Process of Structure-Based Drug Design. *Chem Biol* 10(9):787–797.
645
646 52. Lounnas V, et al. (2013) Current progress in Structure-Based Rational Drug Design marks a
647 new mindset in drug discovery. *Comput Struct Biotechnol J* 5(6):e201302011.
648
649 53. Marshall GR (2012) Limiting assumptions in structure-based design: binding entropy. *J*
650 *Comput Aided Mol Des* 26(1):3–8.
651
652 54. Yoshida H, Bogaki M, Nakamura M, Yamanaka LM, Nakamura S (1991) Quinolone resistance-
653 determining region in the DNA gyrase gyrB gene of Escherichia coli. *Antimicrob Agents*
654 *Chemother* 35(8):1647–50.
655
656 55. Huang X, Zhang A, Chen D, Jia Z, Li X (2010) 4-Substituted 4-(1H-1,2,3-triazol-1-yl)piperidine:
657 novel C7 moieties of fluoroquinolones as antibacterial agents. *Bioorg Med Chem Lett*
658 20(9):2859–63.
659
660 56. Drlica K, et al. (2014) Bypassing fluoroquinolone resistance with quinazolinediones: studies of
661 drug-gyrase-DNA complexes having implications for drug design. *ACS Chem Biol* 9(12):2895–
662 904.
663
664 57. Ahmad Z, et al. (2011) Activity of the fluoroquinolone DC-159a in the initial and continuation
665 phases of treatment of murine tuberculosis. *Antimicrob Agents Chemother* 55(4):1781–3.
666
667 58. Pucci MJ, Ackerman M, Thanassi JA, Shoen CM, Cynamon MH (2010) In vitro antituberculosis
668 activities of ACH-702, a novel isothiazoloquinolone, against quinolone-susceptible and
669 quinolone-resistant isolates. *Antimicrob Agents Chemother* 54(8):3478–80.
670
671 59. Molina-Torres CA, et al. (2014) Intracellular activity of tedizolid phosphate and ACH-702
672 versus Mycobacterium tuberculosis infected macrophages. *Ann Clin Microbiol Antimicrob*
673 13(1):13.
674
675 60. Poissy J, et al. (2010) Should moxifloxacin be used for the treatment of extensively drug-
676 resistant tuberculosis? An answer from a murine model. *Antimicrob Agents Chemother*
677 54(11):4765–4771.
678
679 61. Drlica K, et al. (2009) Quinolones: action and resistance updated. *Curr Top Med Chem*

9(11):981–98.

62. Gentry AC, et al. (2011) Interactions between the etoposide derivative F14512 and human type II topoisomerases: implications for the C4 spermine moiety in promoting enzyme-mediated DNA cleavage. *Biochemistry* 50(15):3240–9.

63. Schneider CA, Rasband WS, Eliceiri KW (2012) NIH Image to ImageJ: 25 years of image analysis. *Nat Methods* 9(7):671–675.

64. Li MZ, Elledge SJ (2007) Harnessing homologous recombination in vitro to generate recombinant DNA via SLIC. *Nat Methods* 4(3):251–6.

65. Kabsch W (2010) XDS. *Acta Crystallogr D Biol Crystallogr* 66(Pt 2):125–32.

66. Kabsch W (2010) Integration, scaling, space-group assignment and post-refinement. *Acta Crystallogr D Biol Crystallogr* 66(Pt 2):133–44.

67. Winn MD, et al. (2011) Overview of the CCP4 suite and current developments. *Acta Crystallogr D Biol Crystallogr* 67(Pt 4):235–42.

68. McCoy AJ, et al. (2007) Phaser crystallographic software. *J Appl Crystallogr* 40(Pt 4):658–674.

69. Emsley P, Cowtan K (2004) Coot: model-building tools for molecular graphics. *Acta Crystallogr D Biol Crystallogr* 60(Pt 12 Pt 1):2126–2132.

70. Adams PD, et al. (2010) PHENIX: a comprehensive Python-based system for macromolecular structure solution. *Acta Crystallogr D Biol Crystallogr* 66(Pt 2):213–21.

71. Painter J, Merritt EA (2006) Optimal description of a protein structure in terms of multiple groups undergoing TLS motion. *Acta Crystallogr Sect D Biol Crystallogr* 62(4):439–450.

72. Painter J, Merritt EA (2006) TLSMD web server for the generation of multi-group TLS models. *J Appl Crystallogr* 39(1):109–111.

73. Schrödinger L (2010) *The PyMOL Molecular Graphics System, Version~1.3r1*.

74. Larkin MA, et al. (2007) Clustal W and Clustal X version 2.0. *Bioinformatics* 23(21):2947–2948.

FIGURE LEGENDS

Figure 1. DNA cleavage by *Mtb* gyrase induced by fluoroquinolones. **A** Fluoroquinolones tested in this study. The constant quinolone core of each drug is highlighted in orange, numbered as shown around C8-Me-moxifloxacin. **B** DNA cleavage assays with full-length *Mtb* gyrase, using wild type (WT – upper gels) and a GyrA A90S (lower gels) sensitizing mutant. Each fluoroquinolone is titrated against a constant amount of protein (125 nM) and supercoiled (SC) plasmid DNA substrate (12.5 nM). The "no protein" control shows the supercoiled substrate DNA, along with a nicked (N) and linear (L) control lanes. Each gel is representative of triplicate data. **C** Graphical analysis of data in **B**. The relative amount of DNA cleavage is plotted as an increase in linear product (obtained by densitometry) compared to the zero drug control as a function of drug concentration. Left panel – WT, right panel – A90S. Data points and error bars represent the mean and standard deviation of triplicate data, respectively.

Figure 2. Structure of the *Mtb* GyrBA core in complex with DNA and moxifloxacin at 2.4 Å. **A** The *Mtb* GyrBA fusion comprises GyrB amino acids 426-675 and GyrA amino acids 2-500. Protein is shown as a surface with one fusion polypeptide in two shades of pink and the second in two shades of blue; darker sections indicate GyrB. DNA is shown in orange, with moxifloxacin as green spheres and magnesium ions in yellow spheres. **B**, **C** and **D** Orthogonal views of the complex in cartoon representation with transparent surfaces, related by indicated rotations.

Figure 3. *Mtb* possesses a naturally-altered hydrogen bond network to the water/magnesium ion bridge. **A** View of the WT *Mtb* GyrBA active site (colored as Figure 2) with bound moxifloxacin (green sticks) and its associated water/magnesium ion ligand (red/yellow spheres). A single active site magnesium ion (lower yellow sphere) also can be seen, and is coordinated by E459, D532 and D534. The covalent Y129 phosphotyrosine linkage is shown as blue sticks. See **Supplementary Figure 3** for

744 representative electron density. **B** Close-up of moxifloxacin bound to WT *Mtb* gyrase, through a
745 bridging magnesium ion, coordinating waters, and adjacent DNA bases. **C** Close-up of moxifloxacin
746 bound to A90S *Mtb* gyrase, showing the increased support of the hydrogen-bonding network by the
747 additional A90S hydroxyl (olive).

748

749 **Figure 4**. Comparison of fluoroquinolone-gyrase interactions. *Mtb* gyrase is colored as per Figure 2.
750 Drugs are shown as green sticks, magnesium ions as yellow spheres and waters as red spheres. Both
751 the bridging magnesium ion and the more distant active site magnesium ion are visible. Simulated
752 annealing F_o-F_c omit maps were generated and are shown for each drug with accompanying
753 magnesium and waters, contoured to 2.8σ. **A** C8-Me-moxifloxacin bound to WT *Mtb* gyrase. *Mtb*
754 residues that interact with the fluoroquinolones are labeled and shown in each subsequent panel.
755 Residues making van der Waals contacts with the C7 group are marked with an asterisk. **B**
756 Moxifloxacin bound to WT *Mtb* gyrase. Also shown is a superposition of moxifloxacin in complex
757 with *A. baumannii* topo IV (28) (PDB: 2XKK, light orange). **C** Ciprofloxacin bound to A90S *Mtb* gyrase,
758 together with a superposition of ciprofloxacin in complex with *S. aureus* gyrase (29) (PDB: 2XCT,
759 yellow). **D** Gatifloxacin bound to WT *Mtb* gyrase. **E** Levofloxacin with WT *Mtb* gyrase and a
760 superposition of levofloxacin in complex with *S. pneumoniae* topo IV (27) (PDB: 3K9F, olive).

761

762 **Figure 5**. Stability of full-length *Mtb* gyrase-fluoroquinolone-DNA cleavage complexes. **A** and **B** Time-
763 courses of linear product loss following dilution of cleavage complexes. “Pre” indicates the DNA
764 content of the reaction prior to dilution. The zero time-point immediately follows dilution. Assay
765 conditions were varied between **A** and **B** to allow for the increased cleavage activity of C8-Me-
766 moxifloxacin. Moxifloxacin was used in both sets of assays as a comparison. Gels are representative
767 of triplicate data. **C** and **D**, graphical analysis of data in **A** and **B**, respectively. The level of linear
768 product (obtained by densitometry) is normalized to the zero time-point and plotted as a function of

769 time. Data points and error bars represent the mean and standard deviation of triplicate data,

770 respectively.

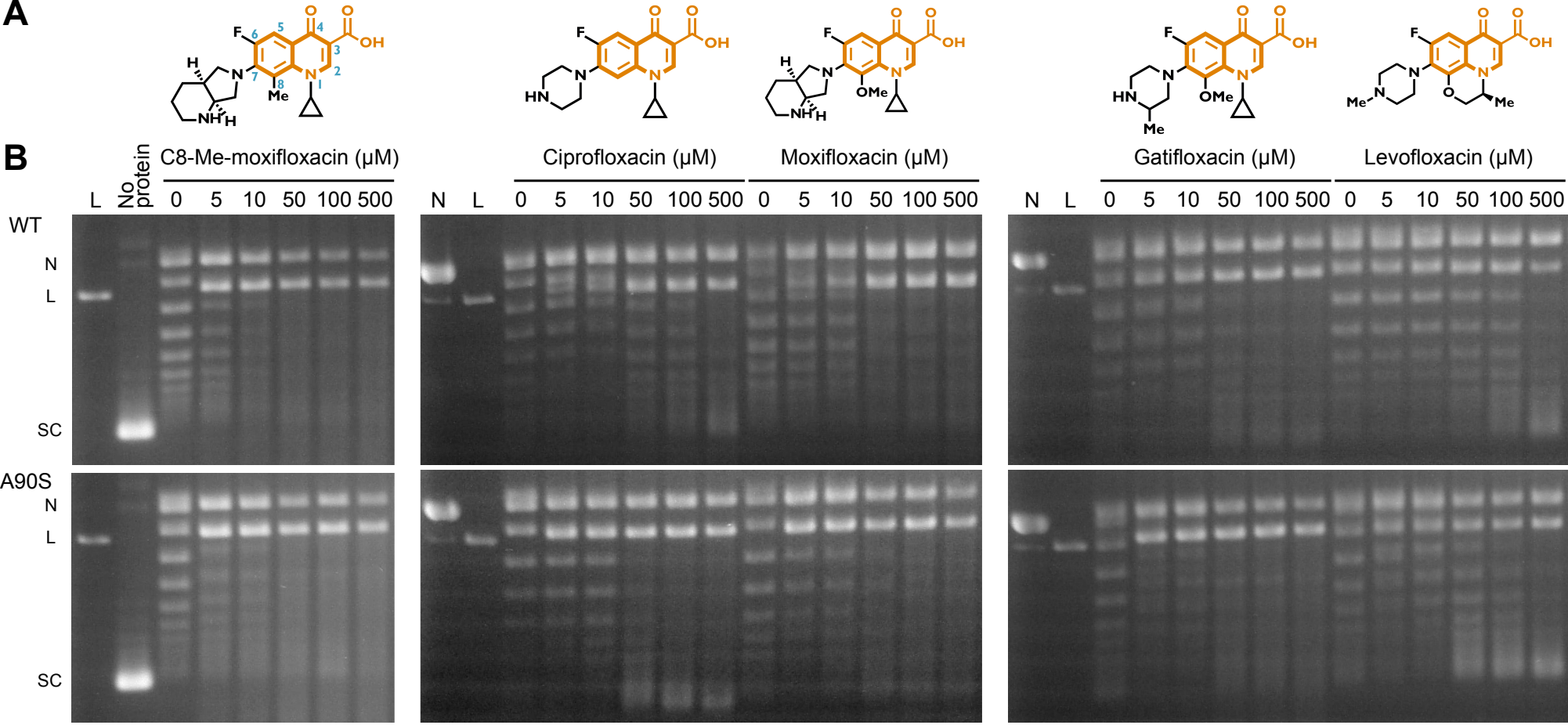
A
B
C8-Me-moxifloxacin (μM)
Ciprofloxacin (μM)
Moxifloxacin (μM)
Gatifloxacin (μM)
Levofloxacin (μM)
No protein
L
N
0 5 10 50 100 500
WT
A90S
SC
C
WT
A90S
Linear product (ΔAU)
Drug concentration (μM)
C8-Me-moxifloxacin
Ciprofloxacin
Moxifloxacin
Gatifloxacin
Levofloxacin

Fig. 1

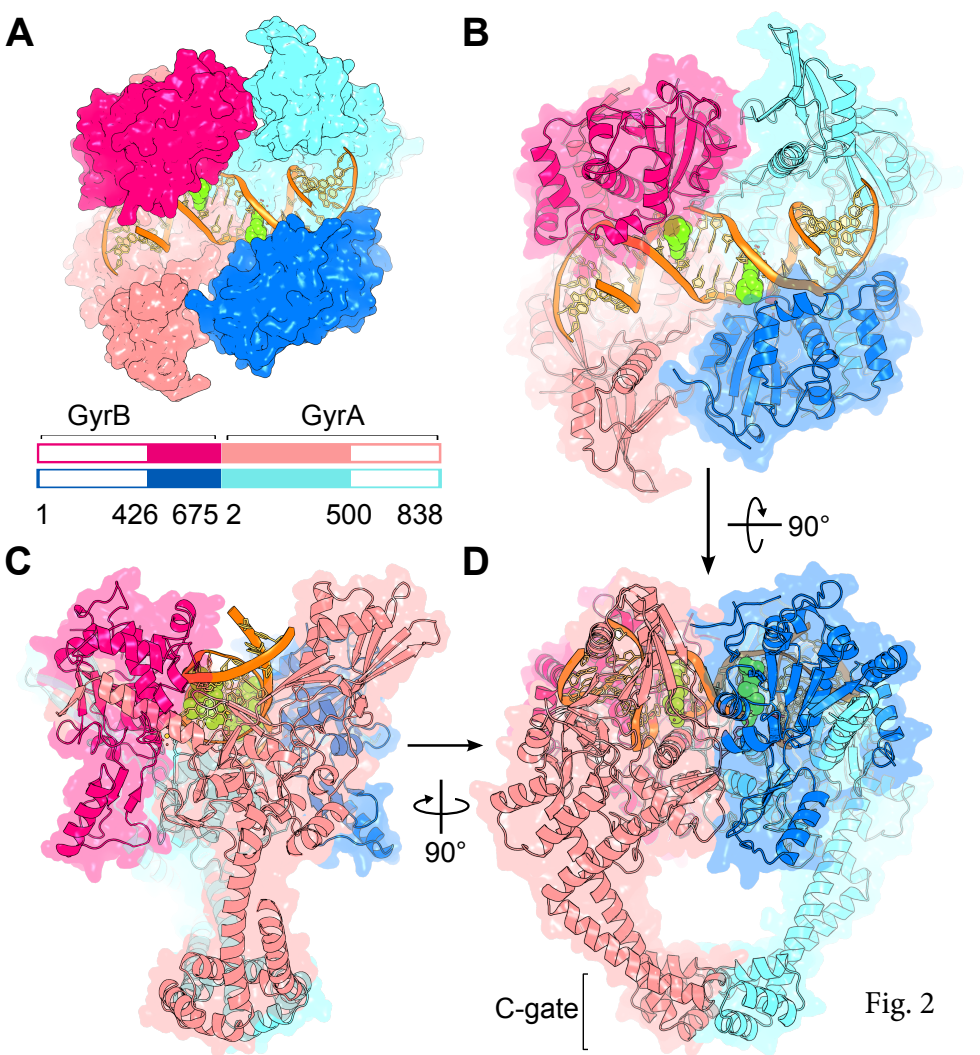

Fig. 2

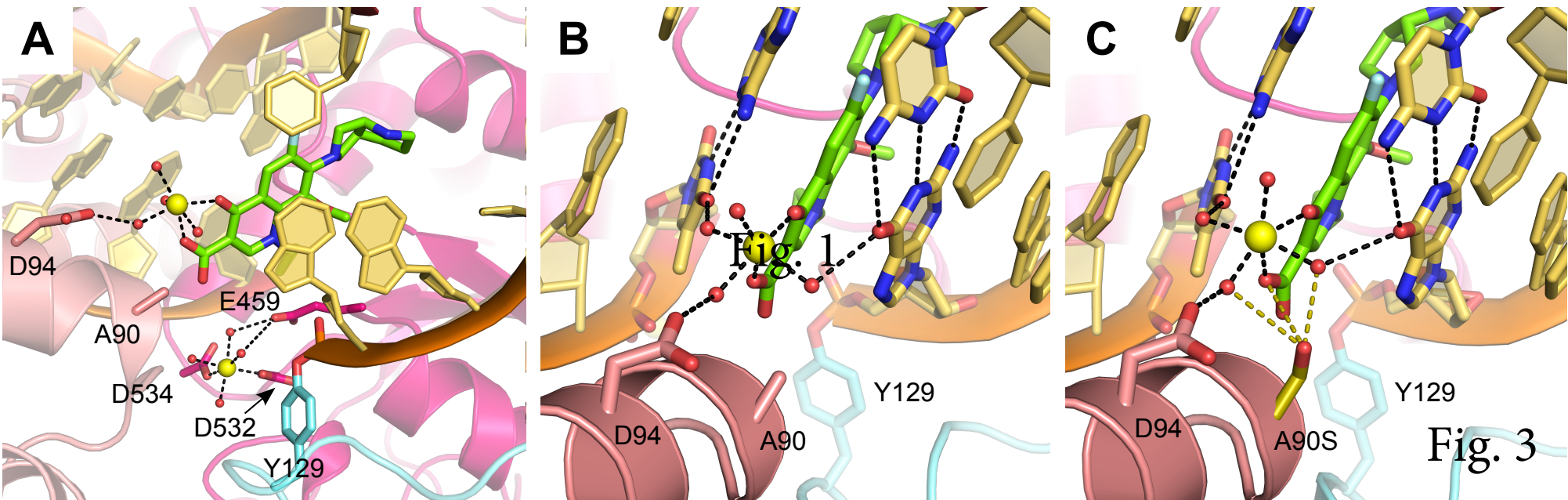
A
D94
E459
A90
D534
D532
Y129
B
Fig. 1
Y129
D94
A90
C
Y129
D94
A90S

Fig. 3

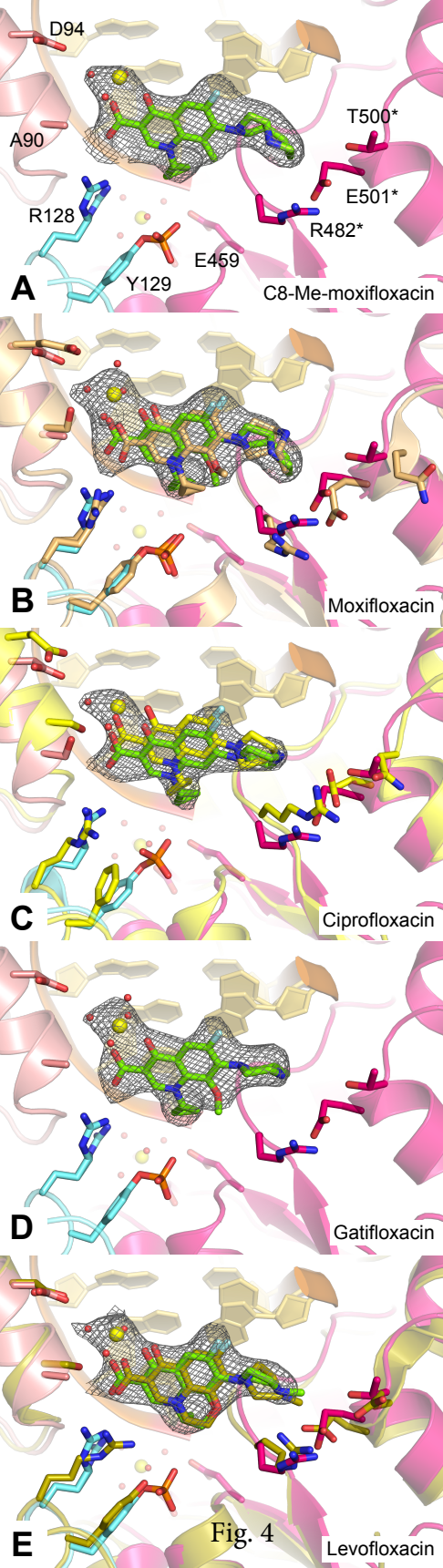
D94
A90
R128
Y129
E459
T500*
E501*
R482*
A
C8-Me-moxifloxacin
B
Moxifloxacin
C
Ciprofloxacin
D
Gatifloxacin
E
Levofloxacin

Fig. 4

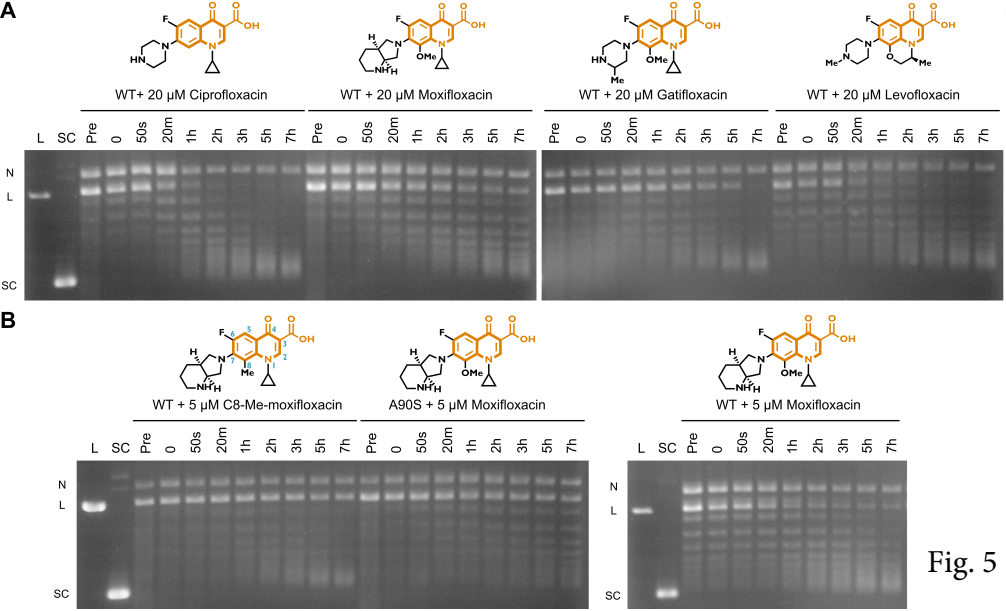
A
WT+ 20 μM Ciprofloxacin
WT + 20 μM Moxifloxacin
WT + 20 μM Gatifloxacin
WT + 20 μM Levofloxacin
L SC Pre 0 50s 20m 1h 2h 3h 5h 7h
N
L
SC
B
WT + 5 μM C8-Me-moxifloxacin
A90S + 5 μM Moxifloxacin
WT + 5 μM Moxifloxacin
C
WT + 20 μM Ciprofloxacin
WT + 20 μM Moxifloxacin
WT + 20 μM Gatifloxacin
WT + 20 μM Levofloxacin
Linear product (%)
Time (hours)
D
WT + 5 μM C8-Me-moxifloxacin
WT + 5 μM Moxifloxacin
A90S + 5 μM Moxifloxacin
Linear product (%)
Time (hours)

Fig. 5

Classification: BIOLOGICAL SCIENCES; Biochemistry

Crystal structure and stability of gyrase-fluoroquinolone cleaved complexes from *M. tuberculosis*

Tim R. Blower[a,1], Benjamin H. Williamson[b], Robert J. Kerns[b] and James M. Berger[a,2]

SUPPLEMENTARY MATERIALS AND METHODS

Cloning. The coding regions for residues 2-675 of GyrB (11, 39) and 2-838 of GyrA from *M. tuberculosis* were amplified from genomic DNA (American Type Culture Collection strain H37Rv) and individually cloned into a pET-28b derivative containing an N-terminal, tobacco etch virus (TEV) protease-cleavable hexahistidine tag. A fusion of GyrB residues 426-675 and GyrA residues 2-500 was formed and cloned simultaneously into a pET-28b derivative containing an N-terminal, TEV protease-cleavable hexahistidine and maltose binding protein tag, using SLIC (64); following TEV protease cleavage, the final protein is left with an extra SNA- sequence at its N-terminus. As part of the cloning procedure for SLIC, the fusions also contained an additional -IGSG sequence at the C-terminus. Mutant vectors were generated by QuikChange (Agilent).

Protein expression and purification. The full-length and fusion proteins were treated similarly, except for an additional ion exchange step for the fusions. Protein was over-expressed in *E. coli* strain Rosetta 2 pLysS (EMD Millipore) by growing cells at 30 °C until early log phase, and then inducing with 1 mM isopropyl-β-D-thiogalactopyranoside for 3 hr. Cells were harvested by centrifugation and resuspended in buffer A500 (20 mM Tris-HCl pH 7.9, 500 mM NaCl, 5 mM imidazole pH 8.0 and 10 % glycerol with protease inhibitors (1 μg/ml pepstatin A, 1 μg/ml leupeptin, 1 mM PMSF)), then frozen dropwise in liquid nitrogen for storage at -80 ˚C.

For protein purification, cells were first thawed, sonicated and centrifuged (17,000 x g, 4 °C). The clarified lysate was next passed over a HisTrap HP column (GE Healthcare) and washed for ten column volumes with buffer A500. At this point, the two procedures diverge for full-length and fusion proteins. Full-length proteins were eluted with buffer B500 (20 mM Tris-HCl pH 7.9, 500 mM NaCl, 250 mM imidazole and 10 % glycerol with protease inhibitors), then concentrated and exchanged into buffer A500 overnight at 4 °C in the presence of His-tagged TEV protease. The fusion proteins bound to the initial HisTrap column were washed for a further 5 column volumes with A100 (20 mM Tris-HCl pH 7.9, 100 mM NaCl, 5 mM imidazole pH 8.0 and 10 % glycerol with protease inhibitors), before elution directly onto a HiTrap Q HP column (GE Healthcare; pre-equilibrated in A100) using B100 (20 mM Tris-HCl pH 7.9, 100 mM NaCl, 250 mM imidazole and 10 % glycerol with protease inhibitors). The Q columns were transferred to an Äkta Explorer (GE Healthcare) and washed with 3 column volumes of A100, then the fusion proteins were eluted using a 50 ml gradient from 100 % A100 to 50 % buffer C (20 mM Tris-HCl pH 7.9, 1 M NaCl and 10 % glycerol with protease inhibitors). The protein peak eluted at approximately 32 % buffer C. Peak fractions were pooled, concentrated and incubated overnight at 4 °C with His-tagged TEV protease.

Following the TEV protease step, all protein mixtures were individually re-passaged over a HisTrap HP column in A500, and the flow-through was collected, concentrated, and run over an S-300 gel filtration column (GE Healthcare) in buffer D (50 mM Tris-HCl pH 7.9, 500 mM KCl and 10 % glycerol). Peak fractions were pooled, concentrated, and when required for biochemistry, diluted into a high-glycerol variant of buffer D, so that the final glycerol concentration reached 30 % prior to aliquotting and snap-freezing in liquid nitrogen for storage at -80 °C. For samples used for crystallography, this protein was dialyzed overnight into buffer E (20 mM Tris-HCl pH 7.9, 150 mM NaCl, 2.5 mM DTT) then quantified and stored on ice for immediate use. If flash-frozen in liquid N_2,

crystallization samples would still form usable crystals over a course of approximately 2-4 weeks of storage.

DNA supercoiling assays. The DNA gyrase holoenzyme was formed by incubating equimolar amounts of GyrB and GyrA (to a final heterotetramer concentration of 10 µm) on ice for 10 min. DNA gyrase was then serially diluted in two-fold steps using protein dilution buffer (50 mM Tris-HCl pH 7.5, 2 mM MgOAc, 1 mM DTT, 500 mM KOAc, 50 µg/ml BSA and 10% glycerol), down to 78 nM. A reaction master mixture was made containing four parts diluted enzyme, five parts 4x reaction buffer (40 mM Tris-HCl pH 7.5, 38.4 mM MgOAc, 4 mM DTT, 100 µg/ml BSA and 32 % glycerol) and one part of a 500 ng/µL solution of relaxed plasmid DNA. The master mixture was incubated on ice for 5 min. Drug titrations were prepared by mixing 2 µL of an appropriate drug dilution (or 2 µL of solvent for "zero drug" controls) with 1 µL of 20 mM ATP and 7 µL of dH_2O. These 10-µL drug mixtures were then added to 10 µL aliquots of the full reaction mixture on ice, quickly transferred to 37 °C, and incubated for 30 min. Final reaction conditions were: 15.6 nM heterotetramer, 12.5 nM relaxed pSG483, variable drug content (or solvent only), 1 mM ATP, 20 mM Tris pH 7.5, 10 mM MgOAc, 1.2 mM DTT, 100 mM KOAc, 35 µg/mL BSA and 10 % glycerol. Following incubation, the reactions were first quenched with 2 µL of stopping buffer (5 % SDS, 125 mM EDTA), followed by adding 1 µL of 12 mg/ml proteinase K and a further incubation at 37 °C for 30 min. Samples were stored on ice until immediately prior to gel loading, whereupon a 6x agarose gel loading dye was added and the samples were warmed to 37 °C for 5 min. Samples were separated by electrophoresis in 1.4 % (w/v) TAE agarose gels (50 mM Tris-HCl pH 7.9, 40 mM NaOAc and 1 mM EDTA pH 8.0 running buffer), for 6-15 h at 2-2.5 V/cm. To visualize the DNA, gels were post-stained with 0.5 µg/mL ethidium bromide in TAE buffer for 30 min, de-stained in TAE buffer for a further 30 min, and exposed to UV illumination.

DNA cleavage assays. DNA cleavage assay were performed largely as per supercoiling assays, with some adjustments: the final concentrations of heterotetramer and fusion homodimer were 125 nM and 250 nM (respectively), negatively-supercoiled pSG483 was used as the substrate, and no ATP was included in the reaction.

Crystallization. The DNA sequence used for crystallization was based upon oligomers that had previously been successfully crystallized by Wohlkonig *et al*. (28). Complementary, non-palindromic 24-nucleotide oligonucleotides with sequences 5'-GGTCATGAATGACTATGCACGTAA-3' and 5'-TTACGTGCATAGTCATTCATGACC-3' were purchased from Integrated DNA Technologies, using the standard purification available. For annealing, oligos, were mixed 1:1 (each at 1.5 mM starting concentration) in water and heated to 95 °C for 5 min in a PCR machine, followed by step decreases of 1 °C per min, to an end-point of 12 °C.

Covalent cleaved complexes were formed by scaling the following 10-µL mixture as appropriate for the number of trays being set. The following reagents were combined in order: 8.3 µL of 6.5 mg/ml GyrBA (in buffer E), 0.4 µL of 100 mM $MgCl_2$, 0.5 µL of 1.5 mM annealed oligos and 0.8 µL of 10 mM fluoroquinolone. For ciprofloxacin, which was dissolved in water rather than DMSO, an additional 0.8 µL of 100 % DMSO was added to the mixture per 10 µL. Once combined, the sample was incubated in a PCR machine at 37 °C for 30 min and then stored on ice until setting trays. Following screening, a single crystal condition was identified in which the resulting complexes formed small showers of crystals. This condition was then refined, producing very thin (<10 µm) planar crystals.

Droplets used to grow data collection-quality crystals were set using a Mosquito robot (TTP Labtech). Hanging drops containing 450 nL complex plus 450 nL reservoir solution were set in 96-well format, using 50-µL reservoirs. A small matrix of 12 crystallization conditions, repeated 8 times throughout the 96-well tray, was used to alleviate batch-to-batch and across-plate variation. The condition matrix used 100 mM Tris-HCl at a varying pH of 7.0, 7.5, 8.0 or 8.5, against 13, 14 or 15 % PEG 4000, with constant 200 mM $MgCl_2$ and 6.25 % PEG 400.

Crystals that formed in these conditions varied widely, from showers to large plates, depending on the protein batch and day. Trays were screened for the larger, planar crystals, which could measure up to 200 µm by 300 µm in surface area, crystals never grew to greater than 10 µm in thickness. Crystals also occasionally grew in clusters that required careful teasing apart during harvesting. To harvest, 20 µL of reservoir was added to 20 µL of cryo buffer (25 mM Tris-HCl pH 7.9, 187.5 mM NaCl, 3.125 mM DTT and 80 % glycerol) and mixed quickly by vortexing; 1 µL of this solution then was added to the 900-nl drop. After addition of cryo buffer, crystals were immediately extracted using a nylon loop and flash-frozen in liquid N_2.

Data collection and structure determination. Initial crystal screening to find suitable crystallization conditions was performed at beamlines 8.3.1 at the Advanced Light Source (Lawrence Berkeley National Laboratory) and X25 at the National Synchrotron Light Source (Brookhaven National Laboratory). The diffraction quality varied greatly not only between crystals but also between different regions of a single crystal. To obtain full data sets with suitable merging statistics, it was necessary to use the microfocus and rastering technologies available at beamlines 23-ID-B and 24-ID-C of the Advanced Photon Source (Argonne National Laboratories) to identify the site at which to collect data. Hundreds of crystals were screened in this fashion to obtain final data sets.

Diffraction data were processed with XDS (65, 66). AIMLESS from CCP4 (67) corroborated the space group as $P2_1$. Initial molecular replacement for the first structure – WT DNA gyrase with DNA and moxifloxacin – was performed using PHASER (68) within CCP4 (67). The search model was a modified version of PDB entry 2XKK (28), with all waters, drug molecules, metals and the phosphotyrosines removed. The obtained solution underwent rigid-body refinement using REFMAC from CCP4 (67). The density maps were examined in COOT (69), which revealed clear difference density of the correct planarity and shape for moxifloxacin. The model was built using COOT and iterative rounds of refinements in PHENIX (70), including the use of TLS parameters (71, 72). Because the DNA substrate was not palindromic, the dsDNA was modelled in both orientations at 50 % occupancy. All ligands were constructed using SMILES strings as input for eLBOW (70); prior to each refinement, the model was prepared using READYSET (70). All loops of the *Mtb* GyrBA fusion were resolved in the structure, with the exception of an initial 5 or 6 amino acid portion of GyrB that forms part of the linker to the missing ATPase domain, and the initial 13 amino acids of GyrA that were co-opted for use as a linker between GyrB and GyrA. The RMSDs between the *Mtb* GyrBA core and the equivalent regions of *A. baumannii* topo IV (28), *S. aureus* gyrase (29) and *S. pneumoniae* topo IV (27) are 1.34, 1.18 and 1.35, respectively. All waters, drug molecules, metals and phosphotyrosines were removed from the final WT-moxifloxacin-DNA structure, to produce the search model for subsequent molecular replacement experiments with all other datasets, which were performed using the PHASER-MR module of PHENIX (70). All final structures contain one cleavage complex in the asymmetric unit and these complexes are essentially C2 symmetric, having 2-fold rotational symmetry. Simulated-annealing omit maps were generated by deleting the drug molecules along with associated magnesium ions and coordinating waters from each model, then running simulated annealing within PHENIX.REFINE (70). Output simulated-annealing maps were then converted using FFT within CCP4 (67). Figures of all subsequent models were generated using PYMOL (73). Alignment of GyrA homologs was generated using ClustalX2 (74).

SUPPLEMENTARY FIGURE LEGENDS

Supplementary Figure 1. Inhibition of full-length *Mtb* gyrase by selected fluoroquinolones. **A** ATP-dependent DNA supercoiling by *Mtb* gyrase, comparing WT (upper gels) and the GyrA A90S mutant (lower gels). Each fluoroquinolone is titrated against a constant amount of protein (15.6 nM) and relaxed plasmid DNA substrate (12.5 nM). The "no protein" control shows the relaxed substrate DNA, along with a nicked (N) and linear (L) control lanes. The constant quinolone core of each drug is highlighted in orange. Each gel is representative of triplicate data. **B** Graphical analysis of data in **A**. Inhibition is measured by the reduction of supercoiled (SC) product (as measured by densitometry) in comparison to the zero drug control as a function of drug concentration. Left panel – WT, right panel – GyrA A90S mutant. Data points and error bars represent the mean and standard deviation of triplicate data, respectively.

Supplementary Figure 2. *Mtb* GyrBA core fusions cleave DNA in the presence of fluoroquinolones. **A** DNA cleavage assays with *Mtb* GyrBA, using WT (upper gels) and the GyrA A90S mutant (lower gels). Each fluoroquinolone is titrated against a constant amount of protein (250 nM) and supercoiled (SC) plasmid DNA substrate (12.5 nM). The "no protein" control shows the supercoiled substrate DNA, along with a nicked (N) and linear (L) control lanes. The constant quinolone core of each drug is highlighted in orange. Each gel is representative of triplicate data. **B** Graphical analysis of data in **A**. DNA cleavage is measured by the increase in linear product (as measured by densitometry) in comparison to the zero drug control as a function of drug concentration. Left panel – WT, right panel – GyrA A90S mutant. Data points and error bars represent the mean and standard deviation of triplicate data, respectively.

Supplementary Figure 3. Detailed structure and electron density of the wild-type *Mtb* GyrBA active site (moxifloxacin-DNA complex). The displayed $2F_o$-F_c electron density maps have been contoured

to 1σ. **A** Moxifloxacin (green sticks), its associated magnesium ion (yellow sphere, upper) and supporting waters are wedged between two bases in the cleaved dsDNA (wheat sticks). The covalent linkage between the DNA and the catalytic tyrosine Y129 (blue sticks) is clearly visible. The single active site magnesium ion (at the non-catalytic "B" position (42)) can also be seen (bottom left). **B** Close-up side view of moxifloxacin, highlighting the unequivocal orientation and position of the drug molecule, together with the drug-bound magnesium atom. At lower contours, evidence can be seen for the solvent-exposed water residues that coordinate the outer edge of the ion. Residues T500 and R482 of GyrB make van der Waals contacts with the C7 ring. **C** Close-up view of the single active site magnesium atom, which also has stronger density for all coordinating water atoms, together with GyrB residues E459, D532 and D534.

Supplementary Figure 4. Overlay of the apo *Mtb* GyrA N-terminal domain structure (PDB: 3ILW) with the structure of *Mtb* GyrBA bound to DNA and moxifloxacin. **A** Detail of the DNA intercalation/bending site. Residues 179-188 of the apo GyrA form are displayed as a green cartoon and apo residues are designated with a prime symbol. The same region in the ternary GyrBA•DNA•moxifloxacin complex is shown as a salmon cartoon. The flexible loop containing I181' forms a β-sheet upon binding DNA, which positions I181 to intercalate and kink the duplex. **B** Detail of the QRDR helix α4, colored as per **A**. D89' in the apo form (purple dots) makes unfavorable contacts with the superposed moxifloxacin. In the presence of moxifloxacin (green spheres), D89 moves and becomes the start of this helix, presenting A90 to the water/magnesium bridge network (magnesium ion, yellow sphere; waters, red spheres).

Supplementary Figure 5. Comparison of electron density around the water/magnesium bridge. The displayed $2F_o$-F_c electron density maps have been contoured to 1σ. **A** WT *Mtb* GyrBA in complex with moxifloxacin (green sticks), bound to GyrA via a magnesium ion (yellow sphere) and its

supporting waters (red spheres). **B** A90S *Mtb* GyrBA in complex with moxifloxacin. In comparison to WT, there is additional electron density linking A90S (olive) to the coordinating water network. **C** Alignment of the GyrA/ParC QRDRs from representative species. The positions of residues 90 and 94 from *Mtb* are indicated. Mtb, *Mycobacterium tuberculosis*; Msmeg, *Mycobacterium smegmatis*; Ecoli, *Escherichia coli*; Abau, *Acinetobacter baumannii*; Saureus, *Staphylococcus aureus* subsp. *aureus*; Spneumoniae, *Streptococcus pneumoniae*; Kpneumoniae, *Klebsiella pneumoniae*; Styphimurium, *Salmonella enterica* subsp. *enterica* serovar *typhimurium*; Lpneumophila, *Legionella pneumophila*; Hpylori, *Helicobacter pylori*. Alignment generated using ClustalX2 (74).

Table S1. Data collection and structure refinement statistics.

	WT•Moxi-floxacin	A90S•Moxi-floxacin	A90S•Cipro-floxacin	WT•Gati-floxacin	A90S•Gati-floxacin	WT•Levo-floxacin	A90S•Levo-floxacin	WT•C8-Me-moxi-floxacin	A90S•C8-Me-moxi-floxacin
PDB ID	5BS8	5BTA	5BTC	5BTD	5BTF	5BTG	5BTI	5BTL	5BTN
Beamline	NE-CAT 24-ID-C	NE-CAT 24-ID-C	NE-CAT 24-ID-C	GM/CA@APS 23-ID-B	NE-CAT 24-ID-C	GM/CA@APS 23-ID-B	NE-CAT 24-ID-C	NE-CAT 24-ID-C	NE-CAT 24-ID-C
Wavelength (Å)	0.979	0.979	0.979	1.033	0.979	1.033	0.979	0.979	0.979
Resolution range (Å)	102.3 - 2.399 (2.485 - 2.399)	49.46 - 2.55 (2.641 - 2.55)	47.7 - 2.55 (2.641 - 2.55)	47.39 - 2.497 (2.586 - 2.497)	49.78 - 2.61 (2.703 - 2.61)	46.33 - 2.5 (2.589 - 2.5)	49.43 - 2.501 (2.591 - 2.501)	49.6 - 2.5 (2.589 - 2.5)	49.65 - 2.5 (2.589 - 2.5)
Space group	$P\ 2_1$	$P\ 2_1$	$P\ 2_1$	$P\ 2_1$	$P\ 2_1$	$P\ 2_1$	$P\ 2_1$	$P\ 2_1$	$P\ 2_1$
Unit cell	108.357 83.07 129.856 90 109.33 90	108.34 83.205 129.757 90 108.55 90	108.336 82.976 129.703 90 109.06 90	107.907 83.158 129.203 90 108.65 90	108.955 84.019 130.59 90 108.87 90	108.094 82.989 129.101 90 108.76 90	108.39 83.28 129.701 90 108.73 90	107.938 83.047 128.737 90 108.88 90	108.337 82.914 129.078 90 108.78 90
Total reflections	289862 (26760)	240848 (23112)	239725 (23493)	285133 (27395)	224023 (21110)	283502 (27762)	253631 (24762)	250735 (22801)	254270 (23071)
Unique reflections	83492 (8068)	69802 (6803)	70181 (6996)	75313 (7331)	66236 (6366)	74925 (7410)	74477 (7351)	73827 (7213)	74277 (7283)
Multiplicity	3.4 (3.3)	3.5 (3.4)	3.4 (3.4)	3.8 (3.7)	3.4 (3.3)	3.8 (3.7)	3.4 (3.4)	3.4 (3.2)	3.4 (3.2)
Completeness (%)	97.68 (93.22)	97.47 (95.53)	98.56 (98.73)	99.66 (97.56)	97.16 (93.62)	99.70 (99.57)	98.14 (97.27)	98.66 (97.11)	98.73 (97.59)
Mean I/sigma(I)	10.66 (0.99)	6.62 (0.66)	8.98 (1.26)	10.36 (1.10)	6.65 (0.86)	8.93 (1.37)	8.92 (1.35)	8.38 (0.91)	8.95 (1.12)
Wilson B-factor	53.37	58.05	50.75	45.59	58.72	40.69	47.9	49.46	47.74
R-merge	0.08799 (1.313)	0.1621 (1.927)	0.1104 (1.06)	0.1365 (1.389)	0.1449 (1.33)	0.1391 (1.061)	0.1072 (0.9755)	0.1335 (1.352)	0.1287 (1.228)
R-meas	0.1043	0.1921	0.1311	0.1593	0.1726	0.1624	0.1274	0.1589	0.1529
$CC_{1/2}$	0.989 (0.52)	0.991 (0.259)	0.995 (0.599)	0.993 (0.365)	0.991 (0.367)	0.991 (0.545)	0.995 (0.562)	0.993 (0.408)	0.993 (0.463)
CC*	0.997 (0.827)	0.998 (0.641)	0.999 (0.866)	0.998 (0.732)	0.998 (0.733)	0.998 (0.84)	0.999 (0.848)	0.998 (0.761)	0.998 (0.796)
R-work	0.1957 (0.3807)	0.2233 (0.3858)	0.2243 (0.3937)	0.2146 (0.3620)	0.2304 (0.3906)	0.2256 (0.3469)	0.2145 (0.3550)	0.2297 (0.3963)	0.2232 (0.3654)
R-free	0.2329 (0.3910)	0.2507 (0.3855)	0.2496 (0.3857)	0.2464 (0.3821)	0.2612 (0.3945)	0.2491 (0.3659)	0.2402 (0.3754)	0.2555 (0.4016)	0.2508 (0.3916)
Number of non-hydrogen atoms	13659	13459	13449	13463	13445	13439	13546	13467	13485
macromolecules	13194	13180	13180	13194	13196	13194	13196	13194	13196
ligands	62	62	52	58	58	56	56	60	60
water	403	217	217	211	191	189	294	213	229
Protein residues	1550	1550	1550	1550	1550	1550	1550	1550	1550
RMS(bonds)	0.004	0.004	0.004	0.004	0.004	0.003	0.003	0.004	0.003
RMS(angles)	0.68	0.75	0.69	0.74	0.70	0.69	0.71	0.68	0.69
Ramachandran favored (%)	96	96	96	96	97	97	96	97	96.6
Ramachandran allowed (%)	4.0	4.0	4.0	4.0	3.0	3.0	4.0	3.0	3.4
Ramachandran outliers (%)	0	0	0	0	0	0	0	0	0
Clashscore	3.03	3.19	3.15	3.03	2.68	3.38	3.54	2.88	3.03
Average B-factor	72	76.7	74.2	64.2	72.8	61.5	67	69.3	67.9
macromolecules	72.6	76.9	74.5	64.6	73.3	61.9	67.1	69.5	68.1
ligands	48.3	57	69.6	43.4	52.4	34.5	41.7	45	64.2
solvent	54.7	68.7	57.7	47.2	45.8	43.7	69.5	64.9	55.4

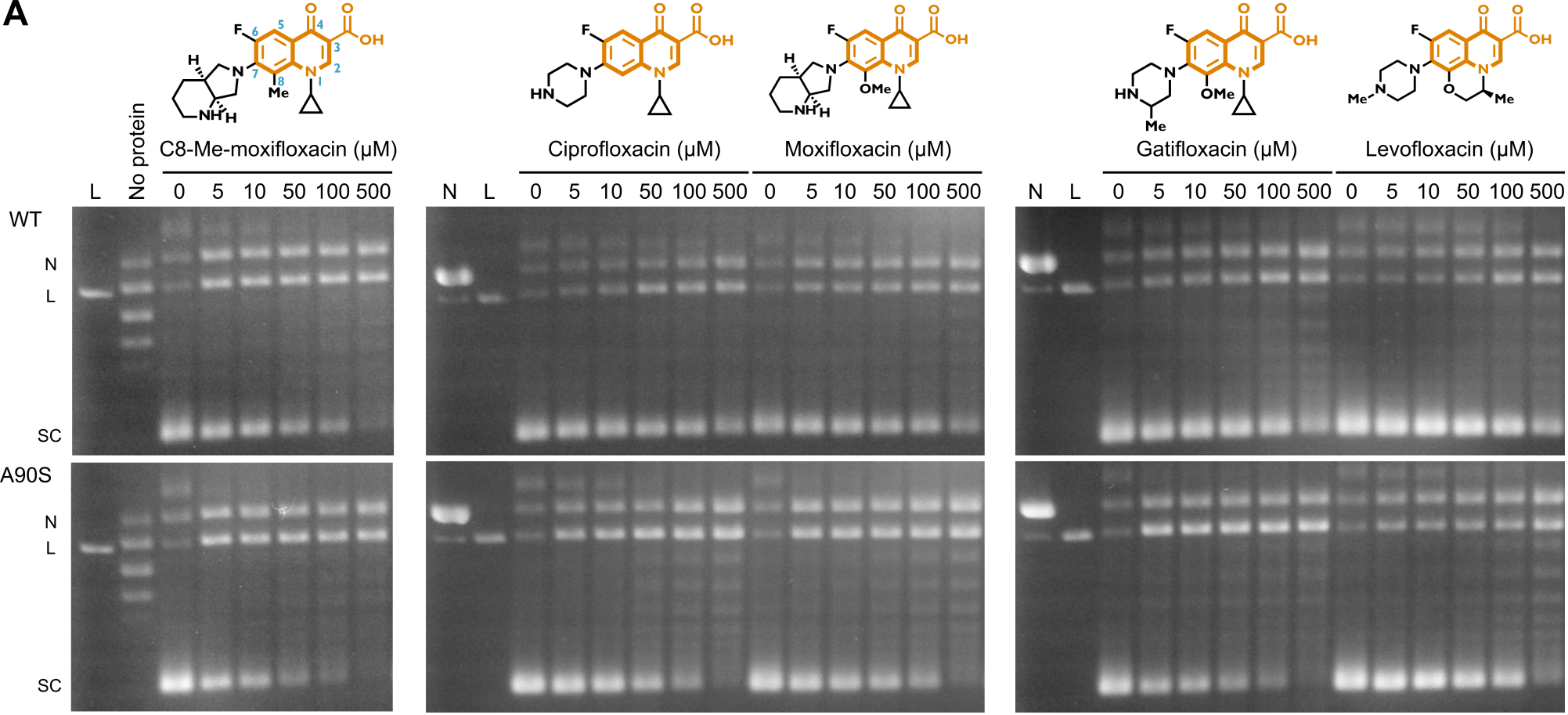
A
No protein
C8-Me-moxifloxacin (μM)
Ciprofloxacin (μM)
Moxifloxacin (μM)
Gatifloxacin (μM)
Levofloxacin (μM)
L
0 5 10 50 100 500
N
L
0 5 10 50 100 500
0 5 10 50 100 500
N
L
0 5 10 50 100 500
0 5 10 50 100 500
WT
N
L
SC
A90S
N
L
SC

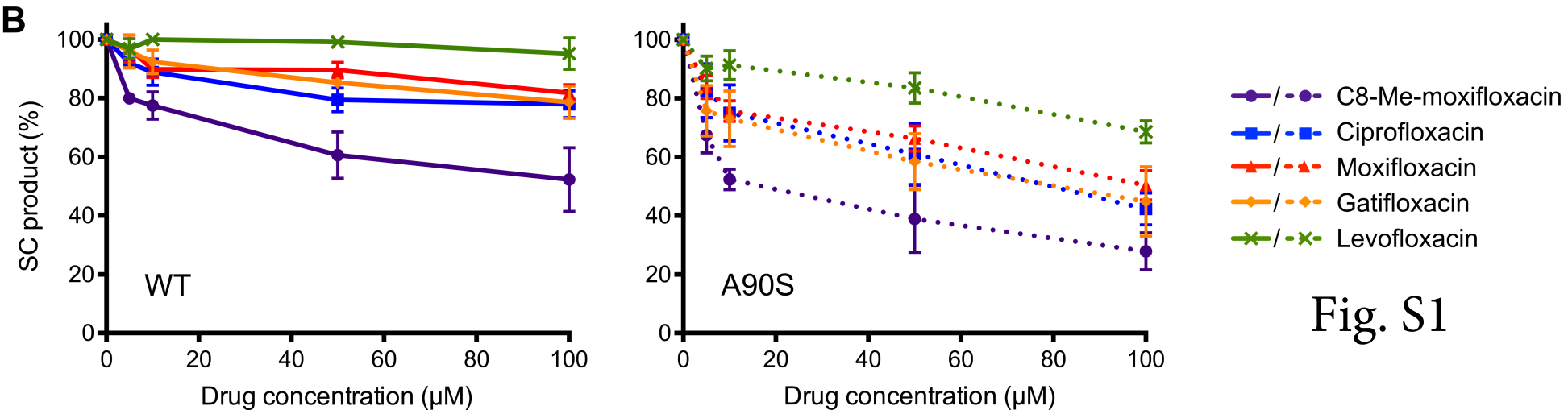
B
SC product (%)
100
80
60
40
20
0
WT
0 20 40 60 80 100
Drug concentration (μM)
A90S
0 20 40 60 80 100
Drug concentration (μM)
C8-Me-moxifloxacin
Ciprofloxacin
Moxifloxacin
Gatifloxacin
Levofloxacin

Fig. S1

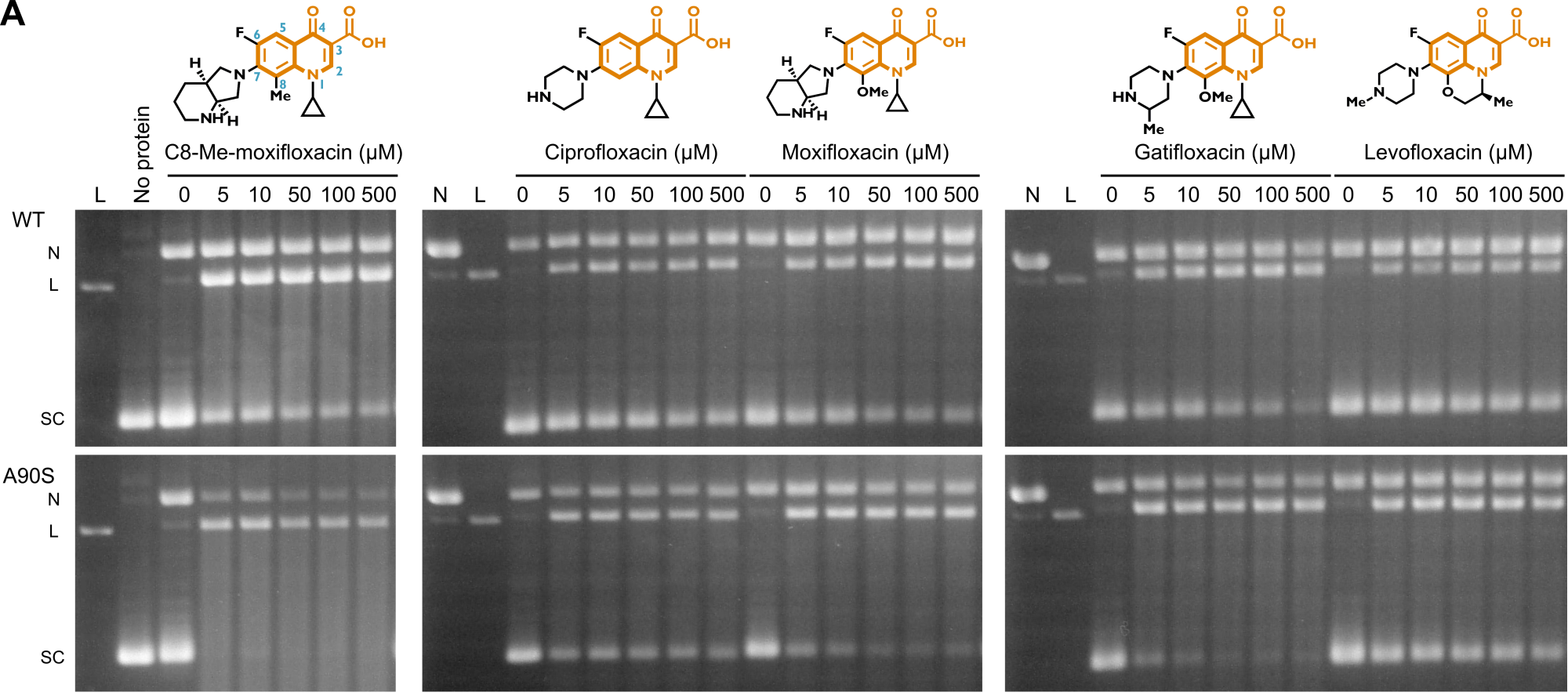
A
C8-Me-moxifloxacin (μM)
Ciprofloxacin (μM)
Moxifloxacin (μM)
Gatifloxacin (μM)
Levofloxacin (μM)
No protein
L
N
0 5 10 50 100 500
WT
A90S
SC

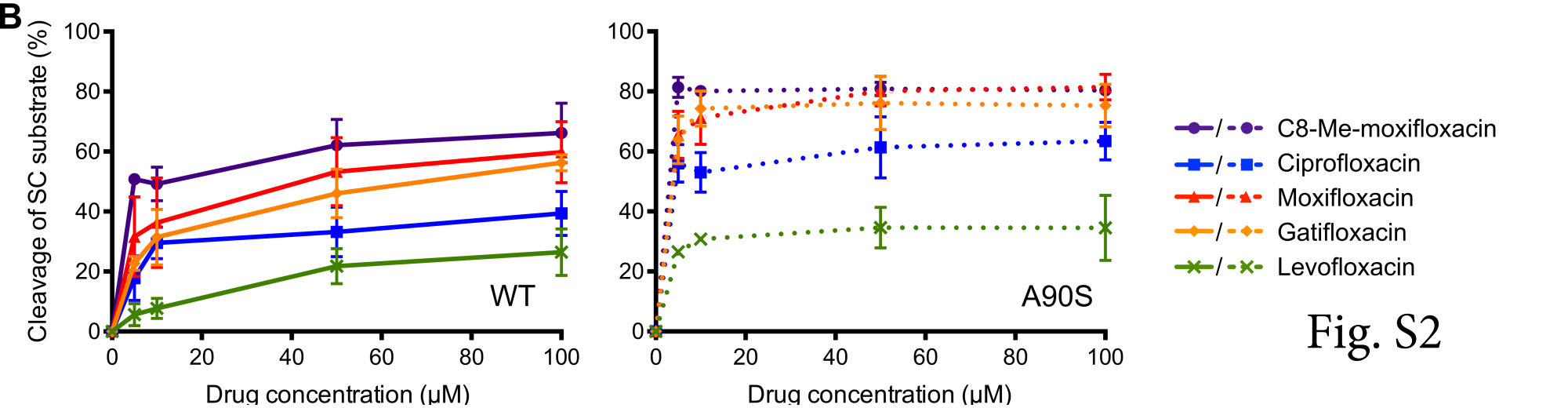
B
Cleavage of SC substrate (%)
Drug concentration (μM)
WT
A90S
C8-Me-moxifloxacin
Ciprofloxacin
Moxifloxacin
Gatifloxacin
Levofloxacin

Fig. S2

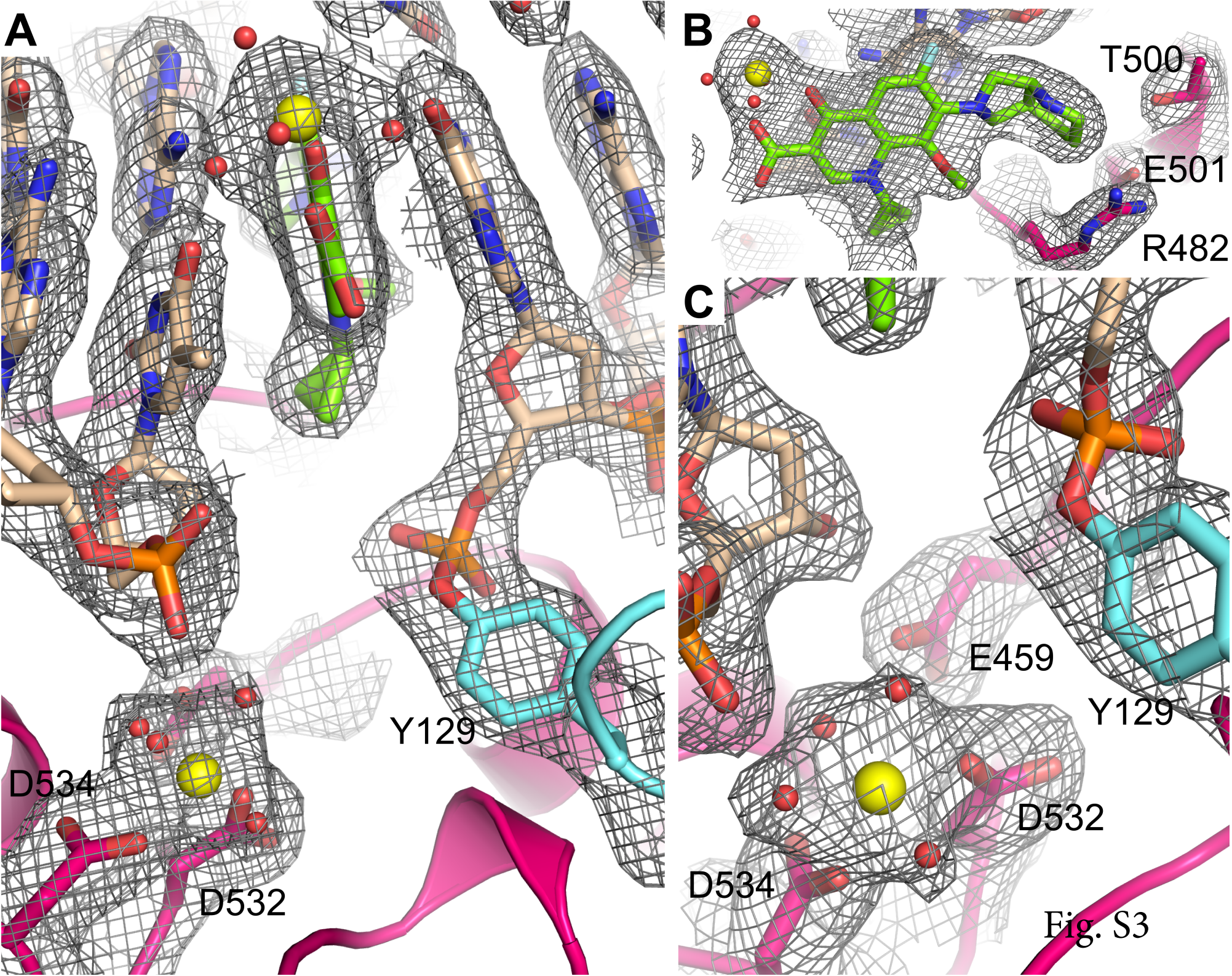

Fig. S3

Fig. S4

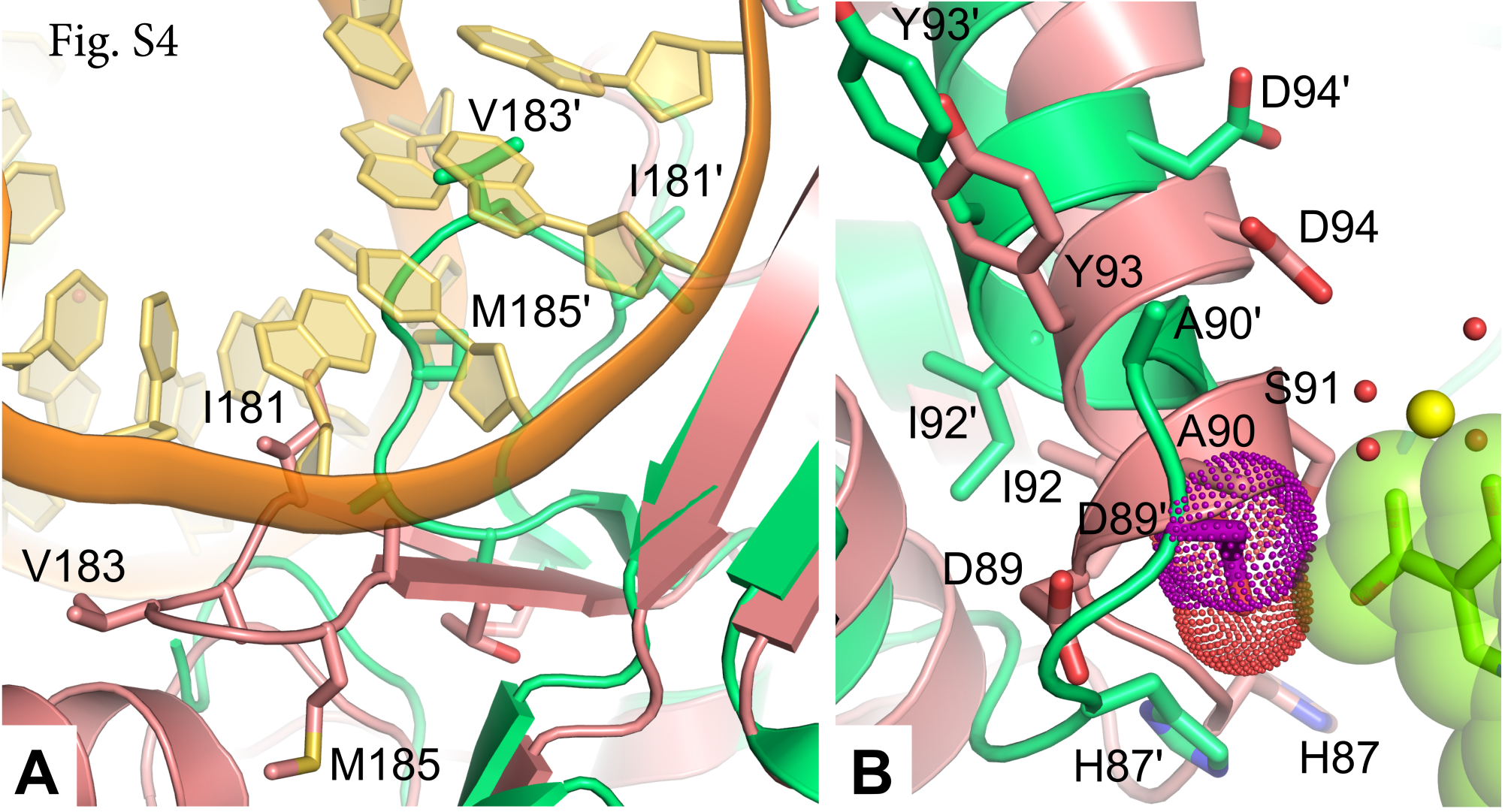
V183'
I181'
M185'
I181
V183
M185
A
Y93'
D94'
D94
Y93
A90'
S91
I92'
A90
I92
D89'
D89
H87'
H87
B

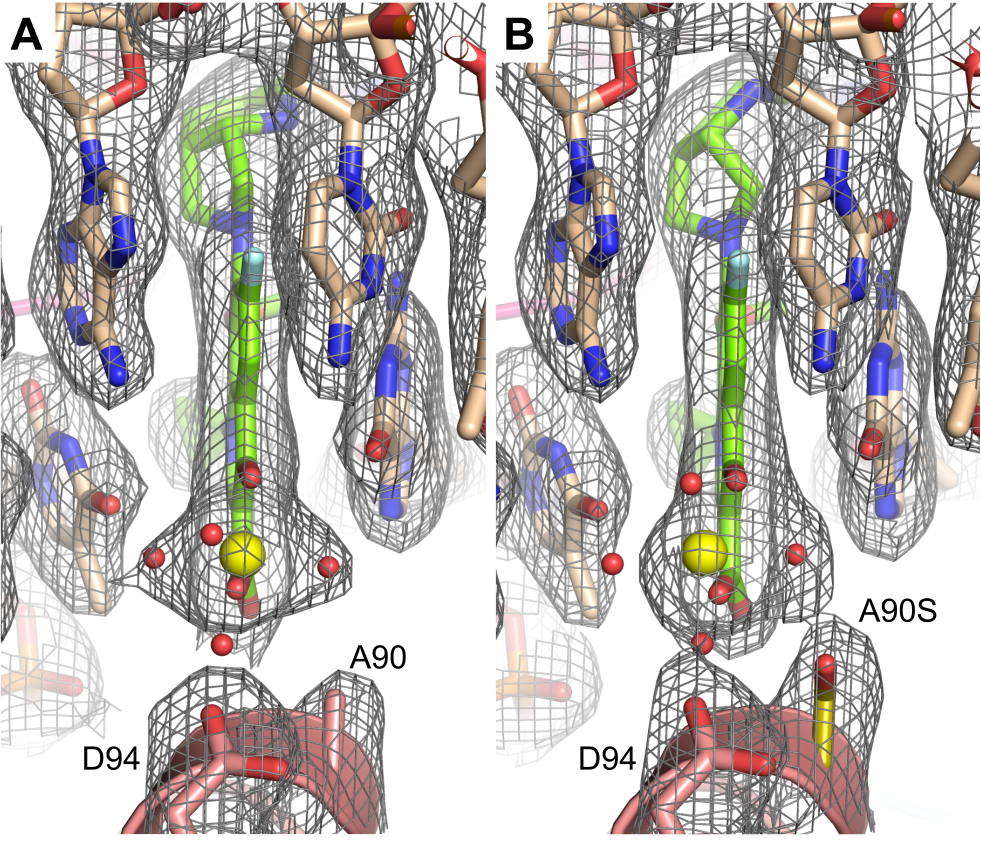

Fig. S5

C

```
                                  90  94
                          :*::***** : *:::* *:* :. *   *:: :** **
Mtb_GyrA                  TMGNYHPHGDASIYDSLVRMAQPWSLRYPLVDGQGNFGSP 119
Msmeg_GyrA                TMGNYHPHGDASIYDTLVRMAQPWSLRYPLVDGQGNFGSP 120
Ecoli_GyrA                VIGKYHPHGDSAVYDTIVRMAQPFSLRYMLVDGQGNFGSI 112
Abau_ParC                 VLGKYHPHGDSACYEAMVLMAQPFSYRYPLIEGQGNWGSP 113
Saureus_GyrA              VMGKYHPHGDSSIYEAMVRMAQDFSYRYPLVDGQGNFGSM 113
Spneumoniae_ParC          IMGNFHPHGDSSIYDAMVRMSQNWKNREILVEMHGNNGSM 108
Kpneumoniae_GyrA          VIGKYHPHGDSAVYDTIVRMAQPFSLRYMLVDGQGNFGSI 112
Styphimurium_GyrA         VIGKYHPHGDSAVYDTIVRMAQPFSLRYMLVDGQGNFGSI 112
Lpneumophila_GyrA         VIGKYHPHGDTAVYDTIVRMAQPFSMRYLLIDGQGNFGSV 112
Hpylori_GyrA              VIGKYHPHGDNAVYNALVRMAQDFSMRLELVDGQGNFGSI 116
```